communications chemistry

A Nature Portfolio journal

Article

https://doi.org/10.1038/s42004-025-01853-z

Chemical and photoinduced interstrand crosslinking of oligo DNA duplexes containing 2′-deoxythioguanosines

Jamila Abbas Osman [1,2], Kazumitsu Onizuka [1,2,3,4] ✉, Yuuhei Yamano [1,2] & Fumi Nagatsugi [1,2,4] ✉

Interstrand crosslinked nucleic acids offer diverse applications, including stabilizing DNA nanostructures in nanotechnology, enhancing miRNA inhibition in therapeutics, and studying enzyme activity in biochemistry. In this study, we present a new crosslinking design strategy that incorporates two 2′-deoxythioguanosine residues at noncomplementary yet strategically proximal positions within an oligo DNA duplex, promoting efficient disulfide crosslinking under chemical oxidation conditions. Additionally, this approach enables a photoinduced crosslinking reaction using 365 nm UV light, further facilitating the formation of disulfide crosslinked duplex. Our results demonstrate that the proximity of reactive thiocarbonyl groups of 2′-deoxythioguanosines incorporated within the duplex favors disulfide bond formation. Herein, we report the design strategy, crosslinking reaction results, and characterization of the crosslinked product. Furthermore, we introduce a new photoinduced disulfide crosslinking reaction and elucidate its mechanism.

The high fidelity of molecular recognition displayed in Watson–Crick base pairing[1] allows oligodeoxynucleotides (ODNs) to recognize their complementary targets in a sequence-selective manner, forming hybridized duplex structures that reversibly dissociate according to thermodynamic principles[2,3]. Beyond this intrinsic sequence specificity, chemical functionalization[4,5] further broadens the utility of nucleic acids by enhancing their thermal stability and resistance to enzymatic processes such as unwinding by helicases[6,7] and cleavage by nucleases[8,9], thereby expanding their applications in nanotechnology, therapeutics, and biochemistry.

Rational chemical functionalization of ODNs with specific functional groups or reactive moieties enables hybridization-specific reactions[10]. By strategically incorporating these groups into modified ODNs, base pairing derived from the assembly of complementary sequences positions reactive sites in close proximity, facilitating and accelerating specific chemical reactions[11]. This approach has been used to create covalently bonded interstrand crosslinked nucleic acid structures, resulting in thermally stable duplexes. These crosslinked nucleic acids have applications in nanotechnology, where they enhance the stability of thermally labile DNA nanostructures[12,13]. They also show promise in therapeutics, particularly as anti-miRNA agents, by improving miRNA inhibition efficiency[14,15]. Additionally, they serve as valuable tools for studying enzyme activity and elucidating molecular mechanisms in biochemistry[16]. Furthermore, they provide deeper insights into biological processes that maintain genomic integrity, thereby aiding investigations into DNA repair mechanisms and cellular responses to DNA damage[17,18].

Various strategies have been developed to achieve interstrand crosslinking within nucleic acids using chemically functionalized ODNs. The introduction of reactive moieties into single-stranded probes enables site-specific crosslinking with unmodified complementary targets through diverse chemical reactions. For example, photo-activated crosslinking reactions have been reported using psoralen[19–21], carbazole[22–25], diaziridine[26,27], chloro-aldehyde[28], coumarin-modified ODNs[29,30], or photocaged nucleobases[31], which can be light-activated to generate interstrand crosslinks with complementary DNA strands. Chemically activated groups, such as furan derivatives undergoing oxidation-based crosslinking[32,33], have also been applied. Our group has previously developed vinyl-mediated Michael-type crosslinking reactions between a reactive base analog and its complementary natural nucleobase[34–37]. Other strategies involve modifying one strand to generate electrophilic intermediates that are subsequently attacked by nucleophilic sites on the complementary DNA strand[38–42].

Alternatively, interstrand crosslinking can be achieved by incorporating reactive groups into each strand of the duplex. Upon hybridization, these groups are brought into close proximity, which allows them to undergo covalent bond formation through well-established chemical reactions such as amide bond formation[43], imine formation[44–46], click reactions[47,48], and photocycloaddition[49–52]. Among these, disulfide bonds—

[1]Institute of Multidisciplinary Research for Advanced Materials, Tohoku University, Sendai, Miyagi, Japan. [2]Department of Chemistry, Graduate School of Science, Tohoku University, Sendai, Japan. [3]Division for the Establishment of Frontier Sciences of Organization for Advanced Studies, Tohoku University, Sendai, Japan. [4]These authors jointly supervised this work: Kazumitsu Onizuka, Fumi Nagatsugi. ✉e-mail: onizuka@tohoku.ac.jp; nagatugi@tohoku.ac.jp

formed by the oxidation of free thiols introduced at opposing positions on complementary ODN strands—enable the controlled and reversible assembly of thio-modified ODNs[53]. Their unique properties, which include relative stability under physiological conditions[54–56], reversibility, and responsiveness to redox environments[57–59], facilitate their application in nanotechnology[60–63], cellular delivery[64], and therapeutic development[65]. For example, DNA structures designed with complementary regions and thiol groups can form mechanically interlocked assemblies via disulfide bond formation[66]. Such mechanically interlocked DNA structures have significant potential in nanotechnology, particularly in constructing DNA-based supramolecular systems. In addition, the fully interlinked structure remains stable unless exposed to reducing conditions, such as the cytosolic environment within cells, where disulfide-linked structures are cleaved, enabling targeted cargo release in drug delivery applications[67]. Furthermore, the reversible nature of disulfide-linked strands can be utilized as a mechanistic probe for studying enzyme activity and molecular interactions within nucleic acid contexts[68]. Grasby et al. introduced reversible interstrand disulfide crosslinks by oxidizing non-Watson–Crick 4-thiouridine (^{4S}U) and 6-thioguanosine (^{6S}G) base pairs incorporated at complementary positions in a double-flap structure (Fig. 1a). This crosslinked structure, cleaved under reducing conditions, was used to validate the proposed mechanism of the FEN enzyme[69].

Previous studies on interstrand crosslinking using thio-modified nucleobases typically involve artificial nucleobases incorporated at complementary positions. Kawai et al. designed a self-complementary DNA strand containing an unnatural nucleoside with a thiophenyl group (^{S}Ph) at the central complementary site within the ODN duplex (Fig. 1b)[70]. Under oxidizing conditions, this duplex formed disulfide crosslinks, which could be reversibly cleaved in reducing conditions. Kondo et al. utilized a self-complementary DNA duplex incorporating consecutive 6-thioguanosine–6-thioguanosine (^{6S}G–^{6S}G) mismatches (Fig. 1c)[71]. Unlike the thiophenyl-containing ODN duplex, these mismatches exhibited resistance to oxidation, requiring metal ions to promote disulfide bond formation. The incorporation of central mismatched thioguanine bases destabilized the duplex, as hydrogen bonding between two thioguanine bases is not expected. This disruption increased nucleobase fluctuations in the central region and disrupted base-stacking order[72]. However, metal ions coordinated with sulfur atoms, restoring base stacking and reducing

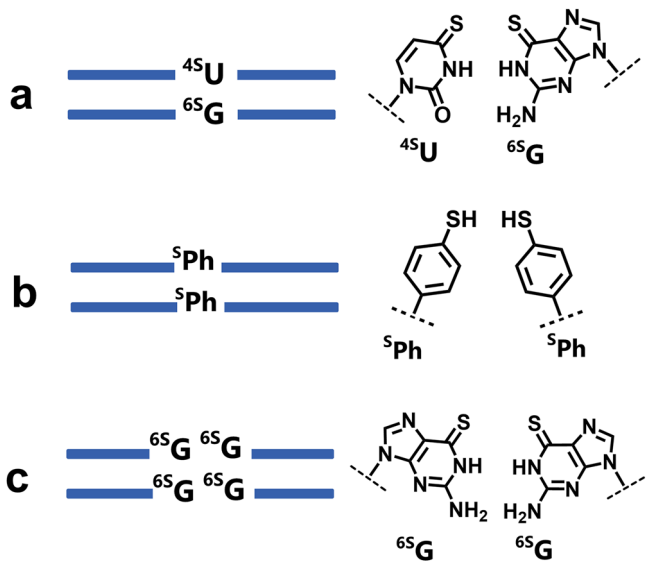

Fig. 1 | Previous studies on disulfide interstrand crosslinking using thio-modified nucleobases or unnatural thiophenyl nucleosides. a Non-Watson–Crick base pairing of 4-thiouridine (^{4S}U) and 6-thioguanosine (^{6S}G), **b** Unnatural nucleoside (^{S}Ph) with a thiophenyl base. **c** Consecutive thioguanosine (^{6S}G) mismatch modifications, all incorporated at complementary position within an oligo duplex.

fluctuations, thereby stabilizing the structure. Therefore, the spatial alignment and proper stacking of thioguanine residues within the duplex structure influence their reactivity. The proximity and conformational preferences of these reactive moieties are critical in determining the efficiency of disulfide bond formation.

In this study, we present a new crosslink design strategy that incorporates two 2′-deoxythioguanosine residues at noncomplementary yet strategically proximal positions within an oligo DNA duplex (Fig. 2). The proposed design establishes an optimal spatial proximity that facilitates interstrand crosslinking, enabling the efficient and straightforward synthesis of disulfide-linked duplex under chemical oxidizing conditions. Notably, it also enables a light-triggered crosslinking reaction upon 365 nm ultraviolet (UV) irradiation, rapidly inducing disulfide bond formation and demonstrating the precise strategic positioning of reactive groups.

Results and discussion

Design and synthesis of oligo DNA duplex incorporating 2′-deoxythioguanosines

The interstrand crosslinking reaction was strategically designed using molecular modeling, which revealed that introducing 2′-deoxythioguanosine (TG) bases into each strand at positions offset by one nucleotide, rather than at complementary sites, positioned the sulfur atoms of opposing TG residues in close proximity (Fig. 2). The modeling further indicated that the formation of a disulfide bond between these closely positioned sulfur atoms would induce only minimal structural changes within the duplex. Based on these insights, we anticipated that a disulfide-crosslinked duplex with minimal conformational alterations could be obtained through a simple chemical modification. Accordingly, the phosphoramidite of 2′-deoxythioguanosine was synthesized following a previously reported procedure[73] starting from commercially available 2′-deoxyguanosine (Scheme S1), then successfully incorporated into oligo DNA using standard solid-phase oligonucleotide synthesis method with an automated DNA synthesizer in DMT-ON mode (Scheme S2), yielding two 12-mer ODN sequences, ODN1 and ODN2 (Table S1) attached to a controlled-pore glass (CPG) solid support. The synthesized ODNs were treated with DBU to remove the 2-ethylhexylpropionate group while still being attached to the CPG resin. The ODNs were then cleaved from the CPG support using an alkaline NaSH solution (Scheme S2) to prevent air oxidation and sulfur loss, resulting in DMTr-protected ODNs. These CPG-cleaved ODNs were subsequently purified by reversed-phase high-performance liquid chromatography (RP-HPLC) (Figure S1a). The 5′-DMTr groups were then deprotected with 5% acetic acid, followed by a second RP-HPLC purification step to remove byproducts formed by air oxidation. (Figure S1b). Matrix-assisted laser desorption ionization time-of-flight mass spectrometry (MALDI-TOF MS) confirmed that the purified ODNs corresponded to the expected sequences. The synthesized oligo DNA strands were designed to form fully matched, complementary duplex incorporating 2′-deoxythioguanosine nucleotides at noncomplementary positions. The resulting duplex was then evaluated for its ability to form disulfide interstrand crosslinks.

Testing of disulfide crosslinking under chemical oxidation

As previously mentioned, the oxidation of thiocarbonyl groups in thio-modified nucleobases to form disulfide linkages within a duplex is known to be accelerated by oxidizing agents such as H_2O_2 or molecular iodine (I_2)[74]. To assess the efficiency of disulfide crosslink formation, we first tested I_2 as an oxidizing agent (Fig. 3a). A reaction mixture containing complementary ODN1 and ODN2 sequences (10 μM each) was incubated with I_2 (100 μM) in phosphate buffer (20 mM, pH 7.0) containing NaCl (100 mM) at 10 °C for 1 h. Denaturing polyacrylamide gel electrophoresis (PAGE) analysis revealed the disappearance of single-stranded ODN bands and the emergence of a high-yield, low-mobility band, indicating efficient crosslinking (Fig. 3b). To evaluate the time dependence of the crosslinking reaction, the reaction was monitored over 1.0–60 min. The results showed that crosslink formation occurred rapidly, reaching high efficiency within 1.0 min of I_2

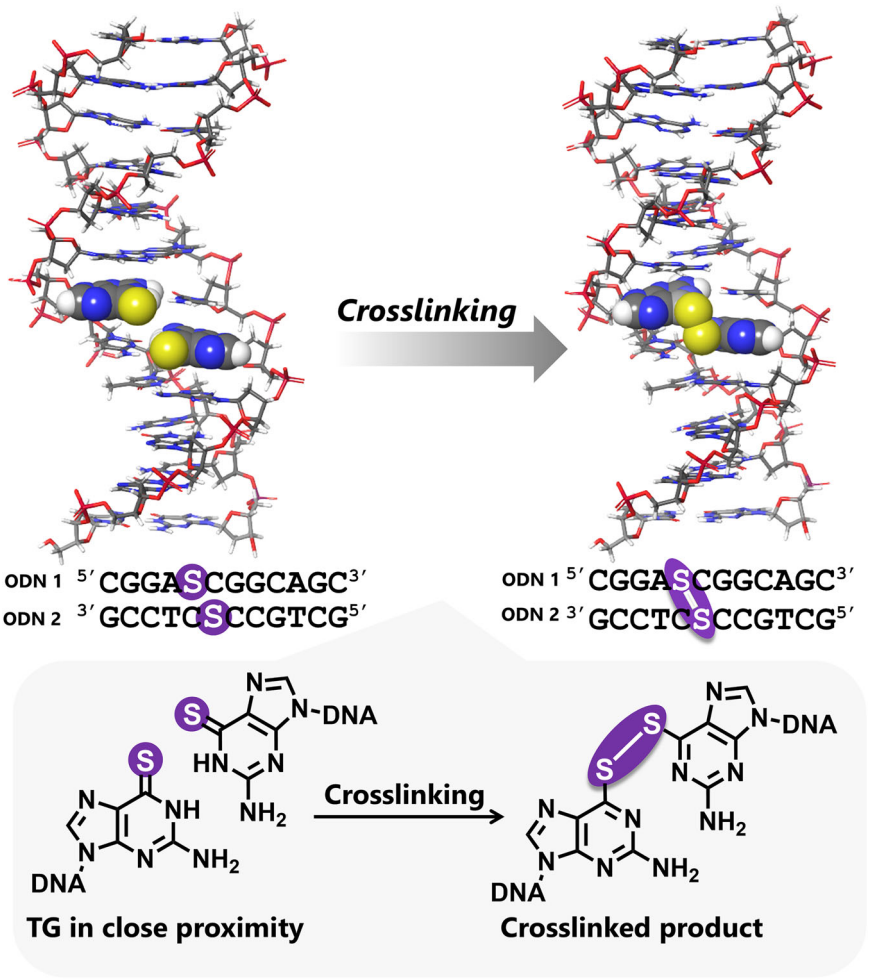

Fig. 2 | Disulfide interstrand crosslinking reaction using 2′-deoxythioguanosine (TG)-containing oligo DNA duplex. Molecular modelling illustrates the incorporation of TG bases (S) at non-complementary yet proximal positions. CPK models highlight TG bases.

incubation (Fig. S2a). The reaction was quenched upon the addition of dithiothreitol (DTT), a reducing agent, at a 2:1 molar ratio relative to I_2, whereas an excess of the oxidizing agent enhanced the crosslinking efficiency (Fig. 3c).

In addition to the single stranded and hetero-crosslinked product bands, faint low-mobility bands were consistently observed by PAGE (Fig. 3). These bands disappeared upon DTT treatment (Fig. 3c), suggesting the presence of self-crosslinked species formed via disulfide bonds. Such self-crosslinking likely arises from a partial self-complementary base pairing that enables transient duplex formation, thereby facilitating intermolecular disulfide homo-crosslinking (Fig. S3a) through slow air oxidation over time. Denaturing PAGE analysis indicated that these self-crosslinked ODNs migrated more slowly than the fully complementary crosslinked duplex, likely due to highly mismatched crosslinked structures that hinder electrophoretic mobility. Notably, these self-crosslinks were readily reduced by DTT, whereas the presence of a complementary strand selectively promoted hetero-crosslinking with the aid of an excess oxidizing agent (Fig. 3c).

To better characterize the self-crosslinked species, HPLC was used to analyze each single-stranded ODN solution, which revealed two distinct peaks A and B (Fig. S3b). Peak B was identified as a self-crosslinked product, as DTT reduction yielded the corresponding single-stranded ODN in PAGE analysis (Fig. S3c), confirming the presence of reversible disulfide bonds. MALDI-TOF MS analysis of peak B predominantly showed reduced single-stranded ODNs due to the cleavage of disulfide bonds during laser desorption/ionization. However, low-intensity signals corresponding to intact self-crosslinked products were also detected (SI, MALDI-TOF MS).

The HPLC-purified hetero-crosslinked product was similarly analyzed by MALDI-TOF MS. As observed for the self-crosslinked species, the spectrum mainly showed peaks corresponding to the reduced single strands (ODN1 and ODN2) with a low-intensity peak corresponding to the intact crosslinked duplex ($[M-H]^-$ calcd for disulfide-crosslinked duplex: 7320.11, found: 7320.32).

The reversibility of the crosslinked adduct was further examined using the reducing agent glutathione (GSH). PAGE analysis revealed that the crosslinked product exhibited concentration-dependent reversibility, yielding two distinct bands corresponding to ODN1 and ODN2 (Fig. S4). These findings confirm the formation of the intended disulfide crosslinked product consisting of ODN1 and ODN2 strands.

Next, we quantified the yield of the disulfide crosslinking reaction. To ensure accurate measurement, pre-existing self-crosslinked ODNs were removed prior to the reaction because they reduced the availability of free thiol groups required for efficient crosslinking. HPLC analysis using ODN1 and ODN2 showed that the crosslinked product was obtained with a 95% yield (Fig. S5), indicating near-quantitative conversion of single-stranded ODNs to the disulfide-linked product.

Overall, our design enables rapid and nearly quantitative interstrand disulfide crosslinking of noncomplementary TG-incorporated residues, achieving a yield of 95% within 1 min under oxidizing conditions.

Testing crosslinking potential under photoirradiation

Unlike native DNA canonical bases, which absorb only UVC and UVB light, thio-modified nucleobases act as UVA-sensitive chromophores that absorb UV light at longer wavelengths. Sulfur substitution at the exocyclic oxygen atoms of the C6 position in purine bases significantly redshifts the lowest-energy absorption band. For instance, 2′-deoxyguanosine has a UV absorption maximum (λ_{max}) of 251 nm, whereas its 6-sulfur-substituted

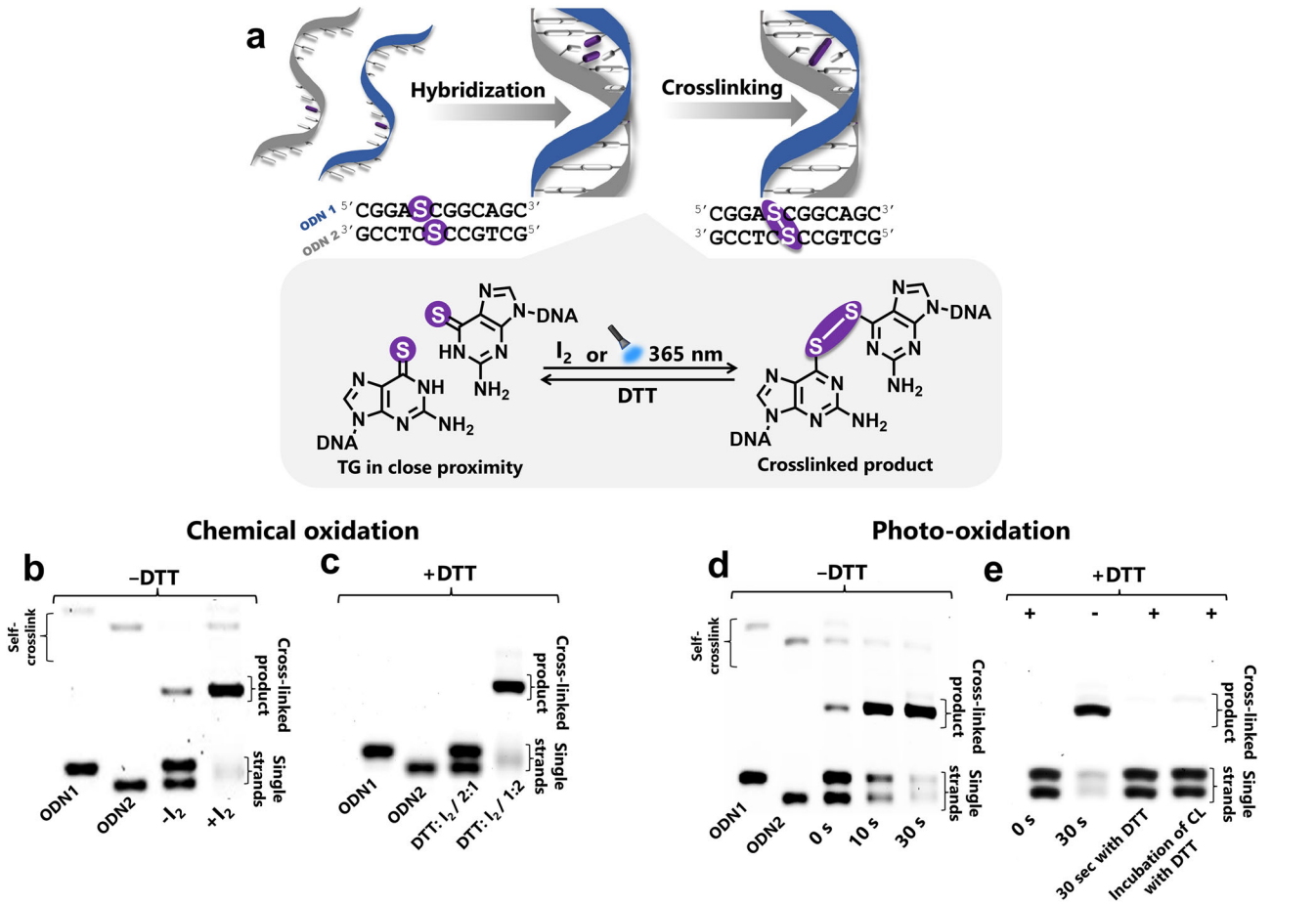

Fig. 3 | Reversible disulfide interstrand crosslinking in 2′-deoxythioguanosine (TG)–containing DNA duplexes. a Schematic representation of the reversible disulfide interstrand crosslinking reaction in TG-containing DNA duplex. Crosslinking is induced under oxidative conditions (either chemically using I_2 or via photoirradiation with 365 nm UV light) and reversed under reducing conditions using DTT. **PAGE analysis of disulfide crosslinking via chemical oxidation**. **b** ODN strands (10 μM each) were prepared in phosphate buffer (pH 7.0, 20 mM) containing NaCl (100 mM) and incubated with oxidizing agent, I_2 (100 μM) at 10 °C for 1.0 h (−DTT condition). **c** ODN duplexes were treated with DTT at a 2:1 (200 μM DTT: 100 μM I_2) or 1:2 ratio (+DTT condition). **PAGE analysis of photoinduced crosslinking**. **d** ODN strands (10 μM each) were prepared in phosphate buffer (pH 7.0, 20 mM) containing NaCl (100 mM) and photoirradiated with 365 nm LED light (UV light intensity: 3.0 W/m²) for 10 s and 30 s at 0 °C (−DTT condition). **e** Duplex photoirradiated for 30 s with DTT (200 μM) or incubated with DTT (200 μM) after 30 s of irradiation (365 nm LED light, intensity: 3.0 W/m²) (+DTT condition). PAGE analysis condition: 16% acrylamide, 20% formamide, and SYBR™ Gold staining.

derivative, 2′-deoxythioguanosine (6-TG), absorbs at a longer wavelength of 341 nm[75]. This shift allows the selective photoactivation of thio-nucleobases under UVA irradiation. Incorporating thio-modified nucleobases into DNA enhances photoreactivity under UVA light, leading to the formation of reactive oxygen species (ROS) and various DNA lesions, including interstrand crosslinks. Notably, 6-TG incorporated into cellular DNA[75–78] has been widely used in photocrosslinking studies involving canonical nucleic acid bases or proteins[79]. Meanwhile, synthetic ODNs incorporating 6-TG are known to form crosslinks with natural pyrimidine nucleobases via a [2 + 2] photocycloaddition reaction, which involves the thiocarbonyl group of 6-TG and the 5,6-double bond of thymine base on the opposite strand[80,81]. Given this well-established photoreactivity, we examined our oligo DNA duplex incorporating 6-TGs under UV irradiation to evaluate its potential for interstrand crosslink formation.

A duplex solution (10 μM of each ODN) in phosphate buffer (20 mM, pH 7.0) containing 100 mM NaCl was photoirradiated with 365 nm UV light at 0 °C for up to 30 s (Fig. 3a). PAGE analysis revealed efficient crosslinking, as indicated by the disappearance of single-stranded ODN bands and the appearance of a high-intensity, low-mobility band corresponding to the crosslinked product (Fig. 3d). To determine the type of crosslink formed, the duplex mixture was irradiated in the presence of DTT (200 μM) or incubated with DTT (200 μM) after photoirradiation. In both cases, the crosslink product band vanished (Fig. 3e), indicating the formation of a DTT-cleavable disulfide crosslink upon photoirradiation. A time-dependent analysis of the crosslinking reaction (Fig. S2b) showed that just 10 s of photoirradiation at a higher light intensity was sufficient to induce efficient crosslink formation. HPLC analysis showed that photoinduced crosslinking between ODN1 and ODN2 achieved a yield of 93% (Fig. S5), which indicates that this method efficiently converts single-stranded ODNs into disulfide-linked duplexes, similar to I_2-induced crosslinking.

MALDI-TOF MS analysis of the HPLC-purified hetero-crosslinked product obtained after photoirradiation revealed peaks corresponding to the reduced single strands (ODN1 and ODN2), along with a low-intensity peak corresponding to the intact crosslinked duplex (SI, MALDI-TOF MS). To further confirm the structure of the photoinduced crosslink, nuclease digestion was performed on the crosslinked duplex, and the results were compared with those of the I_2-mediated crosslink using the I_2 reaction mixture as a positive control. HPLC analysis of the hydrolysates obtained from digested crosslinked duplexes (Fig. 4a) revealed a new peak with a longer retention time alongside peaks corresponding to natural nucleosides (Fig. 4b). Electrospray ionization–mass spectrometry (ESI-MS) analysis confirmed that this new peak matched the mass of disulfide-crosslinked guanosine nucleosides (ESI-HRMS (*m/z*): $[M + H]^+$ calcd for

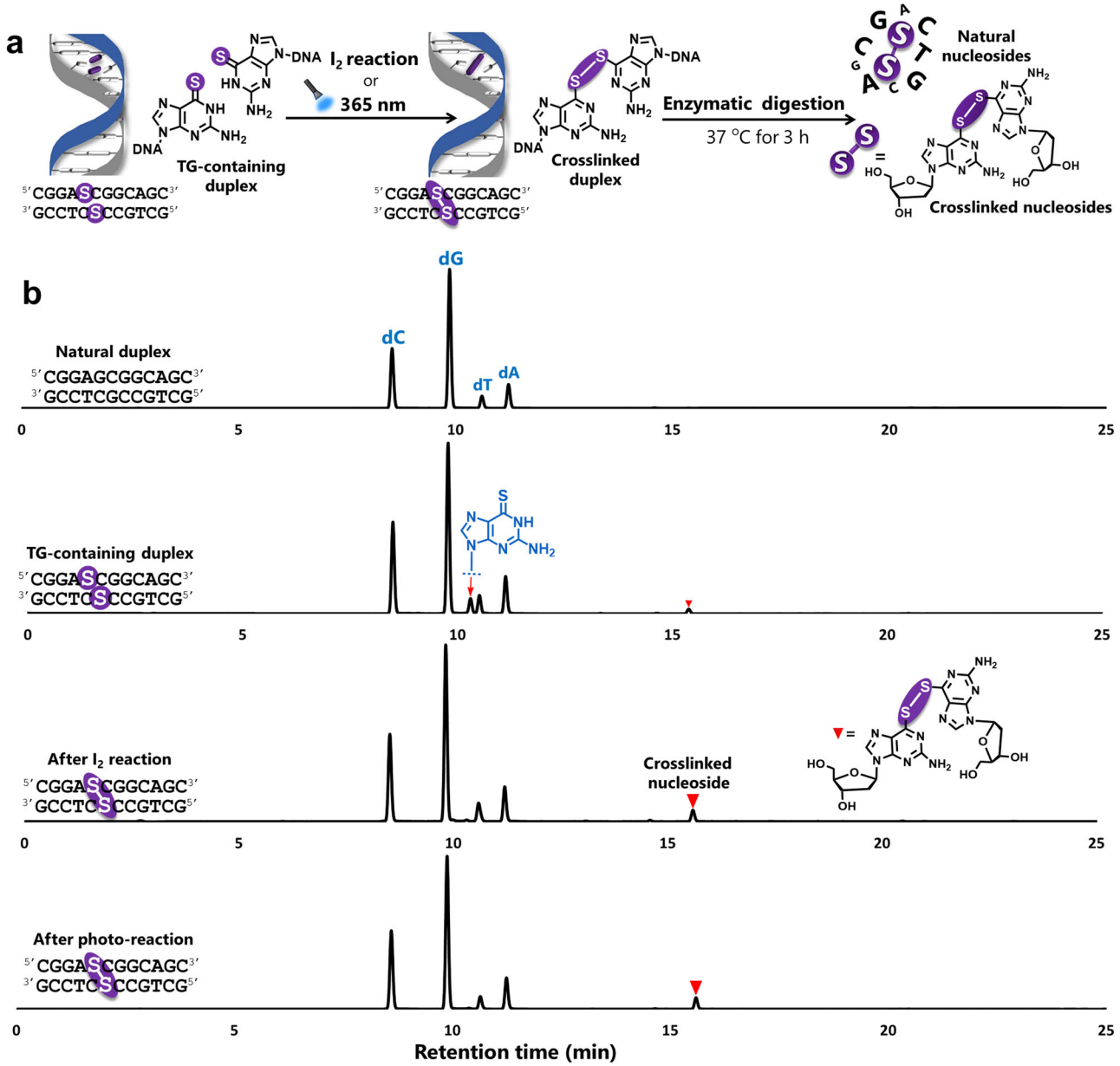

Fig. 4 | Nuclease digestion analysis confirming the structure of the crosslinked product. a Schematic representation of enzymatic digestion experiment for I_2-mediated and photoinduced crosslinked products. The CL product (500 pmol) was incubated with a 10× nucleoside digestion mix reaction buffer and 1× nucleoside digestion mix at 37 °C for 3 h. **b** HPLC analysis followed by ESI-MS analysis of hydrolysates obtained from digested crosslinked duplexes, confirming the mass of disulfide-crosslinked guanosine nucleosides. The chromatograms show retention time (X-axis) from 0 to 25 min, and the peaks correspond to detector response (intensity, Y-axis) monitored at 254 nm, with an approximate signal range of 0–450,000 μV.

$[C_{20}H_{24}N_{10}O_6S_2]^+$: 565.1394, found: 565.1381), verifying the formation of a disulfide crosslink product under both conditions.

Furthermore, the crosslinked product was characterized for its thermal stability and conformational properties. Thermal stability was assessed by measuring the melting temperature (T_m) at 260 nm over a range of 0–90 °C. The crosslinked duplexes exhibited a significant increase in T_m (>80 °C) compared with the noncrosslinked duplex (46 °C) and native duplex (59 °C), indicating enhanced thermal stability due to the covalently linked strands (Figs. 5 and S6). These results confirm the successful formation of the crosslinked product.

To evaluate the conformational effects of incorporating TG residues into precrosslinked and crosslinked oligo DNA duplexes, circular dichroism (CD) spectroscopy was performed. The CD spectra were recorded at 25 °C over a wavelength range of 210–350 nm. Overall, the CD spectra of non-crosslinked and crosslinked duplexes displayed typical B-DNA features, including a positive band around 280 nm due to base stacking and a negative band around 245 nm, characteristic of DNA helicity (Fig. S7), consistent with the right-handed helical structure of B-form DNA[82,83]. An increased intensity of the negative bands in the crosslinked duplexes was observed compared with that in the noncrosslinked duplex, likely due to helical conformational changes induced by covalent linkage formation. These results support the close proximity of the reactive thiocarbonyl groups of TG residues incorporated within our duplex, which facilitates disulfide crosslink formation under oxidative conditions without significantly distorting the B-DNA helix.

Evaluating the applicability of crosslinking design: sequence and orientation dependency

While the inherent reactivity of crosslinking moieties largely defines their potential for crosslink formation, their spatial positioning within the duplex

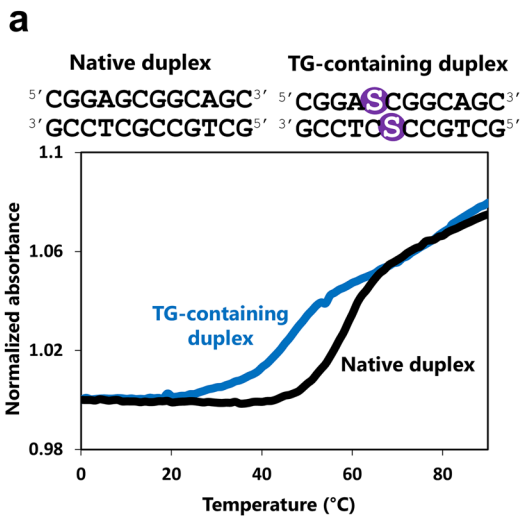

Duplex	T_m (°C)
Native duplex	58.6
TG-containing duplex	46.4

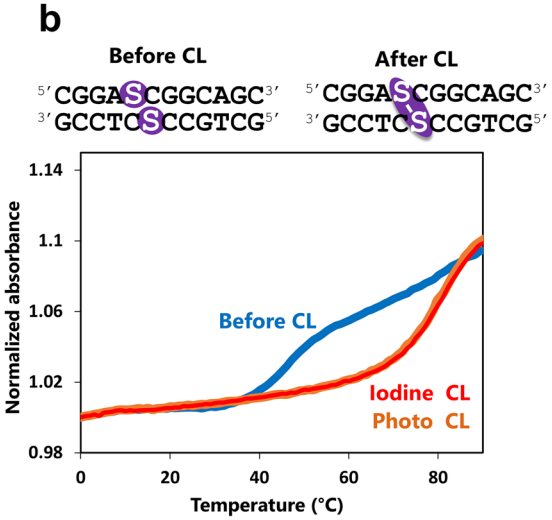

Duplex	T_m (°C)
TG-containing duplex (before CL)	46.4
Iodine CL	**> 80.0**
Photo CL	**> 80.0**

Fig. 5 | Thermal denaturation analysis (T_m measurement). a Comparison of the native duplex and the TG-containing duplex. **b** Thermal stability of the TG-containing duplex before and after the crosslinking reaction. Measurement conditions: T_m was determined by monitoring UV absorption at 260 nm from 0 to 90 °C at a heating rate of 1.0 °C/min. [ODN] = 2.0 μM, [NaCl] = 100 mM, in 20 mM phosphate buffer (pH 7.0).

plays an equally critical role in determining the reaction efficiency. Both the proximity and orientation (angular positioning) of reactive groups are crucial factors for interstrand crosslinking in chemically modified ODNs. Although hybridization templates bring reactive groups into close spatial proximity, ensuring they are within bonding distance[11], proximity alone is insufficient. Efficient crosslinking also requires favorable orientation and proper angular alignment of the reactive moieties to achieve higher reaction rates, greater yields, and improved selectivity for the intended interstrand crosslinking over competing side reactions. Previous studies have shown that inadequate orientation can limit the crosslinking reaction efficiency[45] and yield, or favor side reactions, even when reactive groups are positioned within bonding distance[84–86]. Furthermore, the placement of reactive motifs within the duplex, such as at the terminal or internal positions, and shifting reactive moieties toward the 5′- or 3′-end can influence crosslinking outcomes[38,87–89]. This is because variations in local flexibility, base stacking, and structural constraints affect how readily the reactive groups align and approach their counterparts on the opposite strand, thereby modulating crosslinking efficiency and selectivity. Therefore, designing an effective interstrand crosslinking system with high efficiency, yield, and selectivity requires consideration of both the distance and relative orientation of reactive residues as well as their positional context within the duplex.

To rigorously evaluate the proposed crosslinking strategy—in which TG residues are incorporated at noncomplementary positions—we first examined whether the crosslinking efficiency depends on the TG positions within the duplex when their orientation is maintained as in the original design. Duplexes maintaining the original TG orientation but differing in position were therefore designed (Fig. 6a). In the ODN1-2–ODN2-2 duplex, the TG in ODN1 was shifted three nucleotides toward the 3′ end, while the corresponding TG in ODN2 was shifted equivalently toward the 5′ end. This design positioned the TG residues near the duplex ends and adjacent to a guanine base, creating a local environment different from the original design. Shifting TGs toward the ends placed them in a region that may experience greater local flexibility than the centrally positioned original design. Additionally, this design enabled evaluation of the influence of electron transfer from adjacent bases, particularly guanine. Guanine is the most readily oxidized natural nucleobase and acts as a significant electron donor[90]. It is known to quench the excited state of nearby photoreactive groups through photoinduced electron transfer (PET)[91,92], thereby dissipating energy and reducing the efficiency of the intended photochemical reaction. Therefore, this design allowed us to determine whether the position within the duplex and an adjacent guanine interferes with TG photoexcitation and crosslink formation when the overall orientation is maintained. ODN1-2–ODN2-2 efficiently and selectively produced disulfide-linked products under both chemical oxidation and photoirradiation conditions (Fig. 6b, c). The crosslinked products were fully cleaved with DTT, which confirms the disulfide linkage. Notably, the crosslinking efficiency was comparable to that of the original ODN1–ODN2 duplex, which indicates that maintaining the same orientation of the residues preserved both the reaction efficiency and resulting disulfide-linked product, while the sequence position and adjacency to guanine did not impede reactivity.

Next, we examined whether crosslinking outcomes are affected by the position of TG residues within the duplex: mid-duplex versus terminal. Mid-duplex modifications place reactive residues in a rigid structure stabilized by base stacking, which helps align the reactive groups precisely and promotes selective disulfide formation. In contrast, terminal residues are more flexible, prone to end fraying[93], and more exposed to the solvent, which can destabilize alignment or increase susceptibility to side reactions. To test this, we designed the ODN1-Term–ODN2-Term duplex (Fig. 6a), where TG residues were incorporated at the terminal positions while maintaining the same orientation as in the original design. This duplex formed disulfide crosslinks selectively under both chemical oxidation and photoirradiation (Fig. 6d, e) with only minor formation of DTT-resistant side products under photoirradiation (Fig. 6e). These findings show that, although placing residues at the terminal introduces additional flexibility and potential side reactions, effective and selective disulfide crosslinking is still achievable when the orientation is maintained.

Having established that crosslinking efficiency is not constrained by position, we next aimed to determine if this strategy is limited to a specific alignment or can function across different orientations, which would demonstrate broader potential applicability. Subsequently, we tested the impact of reversing the orientation of the reactive groups by designing a

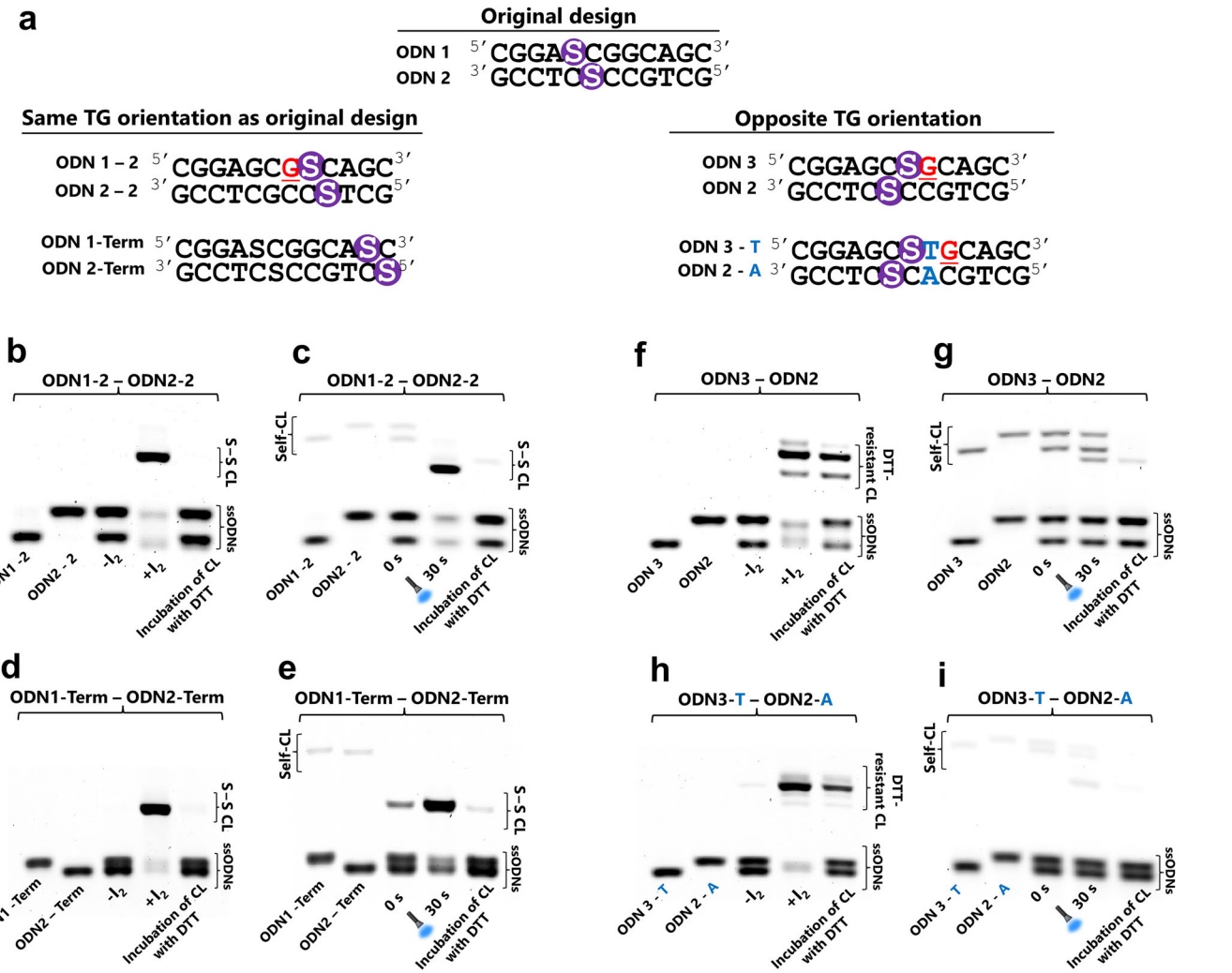

Fig. 6 | Evaluation of positional and orientation effects on disulfide crosslinking in TG-modified DNA duplexes. a Design of duplexes featuring TG residues at various positions and orientations relative to the original ODN1–ODN2 duplex. ODN1-2–ODN2-2 and ODN1-Term–ODN2-Term duplexes retained the same TG orientation as the original design, whereas, ODN3–ODN2 and ODN3-T–ODN2-A duplexes featured the opposite orientation. **b–i PAGE analysis of disulfide crosslinking in TG-modified duplexes under chemical oxidation and photoirradiation conditions**. **b**, **c** ODN1-2–ODN2-2 duplex and **d**, **e** ODN1-Term–ODN2-Term duplex form selective disulfide crosslinks under chemical oxidation and photoirradiation which are fully cleavable by DTT. **f**, **g** ODN3–ODN2 duplex and **h**, **i** ODN3-T–ODN2-A duplex yield mainly DTT-resistant products under chemical oxidation and show no photoinduced crosslinking activity. **Chemical oxidation conditions:** ODN strands (10 μM each) in phosphate buffer (pH 7.0, 20 mM) containing NaCl (100 mM) and DTT (100 μM) were treated with I_2 (200 μM) at 10 °C for 1.0 h. The formed crosslinked (CL) product was incubated with DTT (200 μM) at 10 °C for 30 min. **Photoirradiation conditions:** ODN strands (10 μM each) in phosphate buffer (pH 7.0, 20 mM) containing NaCl (100 mM) were irradiated with 365 nm LED light (UV light intensity: 3.0 W/m^2) for 30 s at 0 °C. The formed CL product was incubated with DTT (200 μM) at 10 °C for 30 min. PAGE analysis condition: 16% acrylamide, 20% formamide, and SYBR™ Gold staining.

duplex featuring an opposite alignment of the reactive TG residues (ODN3–ODN2, Fig. 6a). In this design, the TG position in ODN3 was shifted from the 5th position in ODN1 to the 7th position in the 5′ → 3′ direction, thereby placing the TG residues in an opposite orientation relative to the original ODN1–ODN2 duplex. The ODN3–ODN2 duplex was tested under the same optimized chemical oxidation and photoirradiation conditions as ODN1–ODN2, and the crosslinked products were analyzed by DTT treatment to distinguish disulfide crosslinks from reduction-resistant side products. Unlike the original ODN1–ODN2 duplex, which selectively formed disulfide crosslinks, the crosslinked products of the ODN3–ODN2 duplex were mostly resistant to cleavage by DTT under chemical oxidation (Fig. 6f). Only partial cleavage was observed, indicating that the main products were non-disulfide (DTT-resistant) crosslinks most likely formed through competing reactions, with only minor disulfide formation. Moreover, no crosslinking activity was observed under photoirradiation (Fig. 6g). Given that the ODN3 sequence places a guanine base next to the TG residue, we investigated whether this could account for the lack of photoinduced crosslinking when the orientation was opposite to the original design. To test this, we designed an additional duplex (ODN3-T–ODN2-A, Fig. 6a) with an extra spacer base intended to disrupt possible electronic interactions. However, ODN3-T–ODN2-A exhibited crosslinking behavior similar to that of ODN3–ODN2, mainly forming DTT-resistant products under chemical oxidation along with minor disulfide crosslinking (Fig. 6h) and showed no crosslinking activity upon photoirradiation (Fig. 6i). This suggests that the presence of adjacent guanine is not the main factor suppressing photoreactivity. Instead, the relative orientation of the reactive groups appears to be the key factor influencing the efficiency and selectivity of disulfide crosslink formation.

Overall, these results demonstrate that the efficiency and selectivity of disulfide crosslinking in TG-modified duplexes are strongly orientation-dependent and are governed primarily by the relative orientation of the reactive residues, while not being restricted by the sequence position. Duplexes with opposite alignments yielded predominantly DTT-resistant products and lacked photoinduced crosslinking, whereas maintaining the

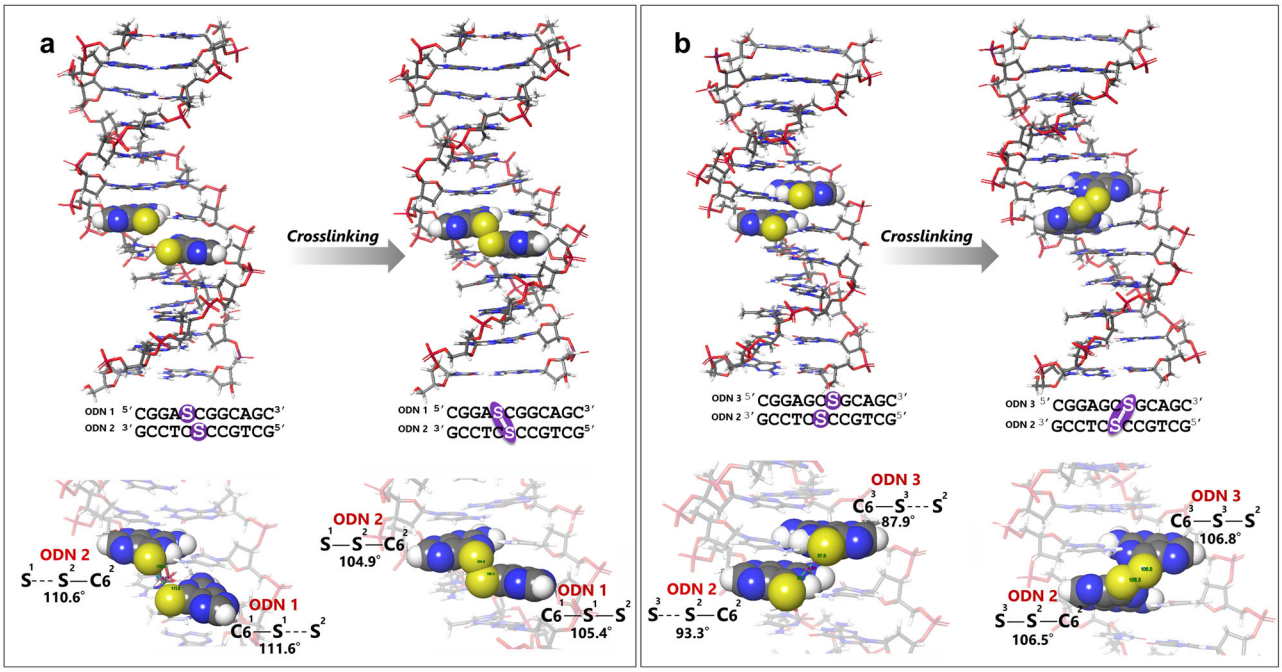

Fig. 7 | Molecular modeling and structural analysis of TG-modified duplexes showing pre- and post-crosslinking geometries and angular reorientation required to achieve the disulfide-linked structures. a ODN1–ODN2 duplex (original orientation) showing near-optimal pre-organization, with minor angular adjustment. **b** ODN3–ODN2 duplex (opposite orientation) showing poor pre-organization, requiring large angular reorientation prior to crosslinking. The CPK models indicate TG bases. The molecular modeling and energy minimization were performed by using MacroModel (Schrödinger). OPLS4 and water were used as the force field and solvent, respectively.

original orientation enabled efficient and selective disulfide formation both at internal and terminal sites. Thus, while flexibility in residue positioning and terminal placement can be tolerated, the strategy remains dependent on maintaining a favorable orientation of TG residues to achieve efficient and selective interstrand crosslinking.

To elucidate the origin of the distinct reactivity observed between the two orientations in disulfide crosslinking, molecular modeling was conducted to evaluate the distance and angular parameters of the disulfide-forming TG residues. The interatomic distance between the sulfur atoms of closely positioned TG residues was calculated to be 4.27 Å in the ODN1–ODN2 duplex (original design) (Fig. S8a) and 4.86 Å in the ODN3–ODN2 duplex (opposite orientation) (Fig. S8b). Although the sulfur atoms in the original design were in closer proximity, this difference ($\Delta = 0.59$ Å) alone is insufficient to explain the contrasting reactivity outcomes. Instead, structural analysis revealed pronounced differences in the conformational changes and angular alignment associated with crosslink formation. The bond angles were measured between the C6–S bonds of each TG and the two sulfur atoms (C6–S···S) in the pre-crosslinking state, and between the C6–S–S bonds in the post-crosslinking state. (Figure S8). In the original design, the angles decreased modestly from 110.6° and 111.6° to 104.9° and 105.4° (Fig. 7a), corresponding to angular adjustments (i.e., change required to achieve the crosslinked geometry) of $\Delta = -5.7°$ and $-6.2°$, respectively. Thus, the initial geometry (average 111.1°) was already close to the final crosslinked angle (average 105.2°). This minor reorientation (average 6.0°) indicates that the duplex was pre-organized for the crosslinking reaction, requiring only a minor conformational adjustment to reach the transition state, thereby lowering the activation energy for bond formation. Consequently, this design efficiently produced disulfide crosslinks under chemical oxidation and photoirradiation conditions.

In contrast, the opposite-direction design displayed notable angular changes from 93.3° and 87.9° to 106.5° and 106.8°, respectively, after crosslinking (Fig. 7b). These correspond to significant increases of $\Delta = +13.2°$ and $+18.9°$, respectively. The initial geometry (average 90.6°) was far from the final disulfide-linked angle (average 106.7°), which indicates that the duplex is poorly pre-organized for the crosslinking reaction. Consequently, a major conformational adjustment and substantial reorientation (average 16.1°) were required prior to bond formation, which resulted in a higher transition energy barrier that was unfavorable for direct disulfide formation. As a result, the reaction was diverted toward unexpected reaction pathways where the slower formation of S–S bonds allowed competing reactions to take place, resulting mainly in DTT-resistant crosslinked products. Under chemical oxidation conditions, disulfide-linked species were formed only as minor products, and no disulfide crosslink formation was observed upon photoirradiation.

Taken together, these results indicate that the near-optimal pre-organization in the original design facilitated efficient and selective disulfide crosslinking, whereas the poor pre-organization in the opposite design required a substantial conformational reorientation that raised the activation barrier and led to inefficient disulfide crosslink formation. Thus, the efficiency and selectivity of disulfide crosslinking in TG-modified DNA duplexes are governed primarily by the relative orientation of the reactive residues rather than their exact sequence position. Therefore, this strategy offers a broad scope with respect to sequence context and residue positioning provided that the favorable orientation of TG residues is maintained.

Elucidating photoinduced crosslinking reaction mechanism

Thio-modified nucleobases exhibit high intersystem crossing (ISC) rate constants (transition from the singlet state to the triplet state) upon UVA exposure, with the triplet state displaying high photoreactivity[94] (Scheme 1 and Eq. 1) due to thiolation that stabilizes sulfur electronic excitation, enabling thiobases to act as photosensitizers, generate ROSs, and enhance photoreactivity toward various photochemical reactions. An important consideration is that 6-TG exhibits context-dependent photochemical reactivity upon UVA irradiation, with the resulting products varying significantly depending on its molecular environment—whether as a monomer or incorporated into synthetic ODNs. Several studies[95–98] have demonstrated that singlet oxygen ($^1O_2$) is the primary ROS generated upon UVA irradiation of 6-TG. This occurs via a type II photosensitization

pathway, where energy transfer from triplet 6-TG (^{3}TG) to ground-state oxygen ($^3O_2$) produces $^1O_2$ (Eq. 2). However, ^{3}TG may also lose energy via electron transfer to $^3O_2$, generating superoxide radicals ($O_2^{\bullet-}$), a process favored in the presence of an electron donor (D) (Eq. 3)[99,100]. This reaction forms $TG^{\bullet-}$ and $D^{\bullet+}$, with $O_2^{\bullet-}$ expected to arise via electron transfer from $TG^{\bullet-}$ to $^3O_2$, regenerating the ground-state TG (^{0}TG).

While the type II photosensitization pathway and its products are well-reported, there are remarkably few studies on type I photosensitization—where electron transfer generates $O_2^{\bullet-}$. Despite the well-known and diverse photochemical reactivity of 6-TG, no previous study, to our knowledge, has clearly demonstrated photoinduced disulfide bond formation between two 6-TG nucleobases incorporated within an oligo DNA duplex. Accordingly, we aimed to elucidate the mechanism underlying disulfide crosslink formation under photoirradiation and to determine whether type I or type II photosensitization predominates in this photochemical reaction system.

To explore our reaction system, we proposed a speculative mechanism (Fig. 8) in which UV irradiation of the oligo DNA duplex incorporating 6-TGs induces charge separation via a single electron transfer (SET) process. Upon photoexcitation, TG on one strand transitions to its triplet excited state (^{3}TG), making it more redox-active than its ground state and allowing it to act as an electron acceptor[101,102]. Meanwhile, ^{0}TG on the opposite complementary strand serves as an electron donor. The strong reducing nature of the sulfur atom in 6-TG facilitates this process[103], resulting in the formation of a radical anion ($TG^{\bullet-}$) at the acceptor site and a radical cation ($TG^{\bullet+}$) at the donor site. Although charge recombination, which regenerates neutral ^{0}TGs, is possible, this process is suppressed under air-saturated conditions due to the abundance of $^3O_2$. Instead, $TG^{\bullet-}$ acts as a type I photosensitizer, transferring an electron to $^3O_2$ to produce $O_2^{\bullet-}$ and regenerate ^{0}TG. Simultaneously, $TG^{\bullet+}$ undergoes deprotonation to form a neutral thiyl radical ($TG^{\bullet}$), which then reacts with ^{0}TG via homolytic cleavage of the thiocarbonyl double bond, leading to the formation of a disulfide-crosslinked adduct. This process generates a carbon-centered radical that delocalizes on the purine ring of the 6-TG base. Incorporation of oxygen, derived from either $O_2^{\bullet-}$ or $^3O_2$ generates a peroxyl anion ($-OO^-$) or peroxyl radical ($-OO^{\bullet}$), which eventually loses a proton, yielding a stable disulfide-crosslinked structure within the DNA duplex.

Based on this hypothesis, we identified four key elements underlying the proposed mechanism. First, $^3O_2$ plays a critical role in the electron transfer step, driving the reaction toward the formation of the crosslinked product. Second, the electron transfer step results in the formation of $O_2^{\bullet-}$ as ROS via a type I photosensitization pathway. Third, the reaction is initiated by SET and subsequent charge separation, facilitated by the close proximity of reactive thioguanosines within the duplex structure. Finally, a thiyl radical intermediate is generated, enabling the crosslinking reaction.

To evaluate the plausibility of the proposed mechanism, we first examined the effect of $^3O_2$ on the reaction efficiency by performing the reaction under an argon atmosphere (Figs. 9a and S9). Using a sealed reaction tube flushed with argon, the samples were irradiated with 365 nm light. PAGE analysis (Fig. 9b) revealed a significant reduction in reaction efficiency under these conditions, as evidenced by a notable decrease in the band intensity of the crosslinked product compared with that observed under air-saturated conditions. These findings highlight the crucial role of $^3O_2$ in driving the photoinduced disulfide crosslinking reaction and enhancing its efficiency. The abundance of $^3O_2$ suppresses charge recombination, thereby promoting crosslink formation, whereas low $^3O_2$ levels allow the recombination of charged radical species, regenerating neutral ^{0}TGs and ultimately reducing the overall reaction efficiency.

$$^0TG \xrightarrow{UVA} {}^1TG \xrightarrow{ISC} {}^3TG \qquad \text{Eq (1)}$$

$$^3TG + {}^3O_2 \xrightarrow{\text{Energy transfer}} {}^0TG + {}^1O_2 \qquad \text{Eq (2)}$$

$$^3TG \xrightarrow[e^- \text{ transfer}]{D \quad D^{\bullet+}} TG^{\bullet-} \xrightarrow[e^- \text{ transfer}]{{}^3O_2} {}^0TG + O_2^{\bullet-} \qquad \text{Eq (3)}$$

Scheme 1 | UVA-induced excitation of thioguanosine (TG) and its Type I/Type II ROS-generating Pathways. Eq. (1) Upon UVA irradiation, ground-state thioguanosine (^{0}TG) is excited to the singlet state (^{1}TG), which undergoes an intersystem crossing (ISC) to the excited triplet state (^{3}TG). Two possible pathways of ^{3}TG to generate ROS in the presence of $^3O_2$, Eq. (2) ^{3}TG can transfer energy to $^3O_2$, generating $^1O_2$ via a type II reaction. Eq. (3) Alternatively, electron transfer from ^{3}TG to $^3O_2$ can produce $O_2^{\bullet-}$ in a type I reaction, a process that is favored in the presence of electron donors.

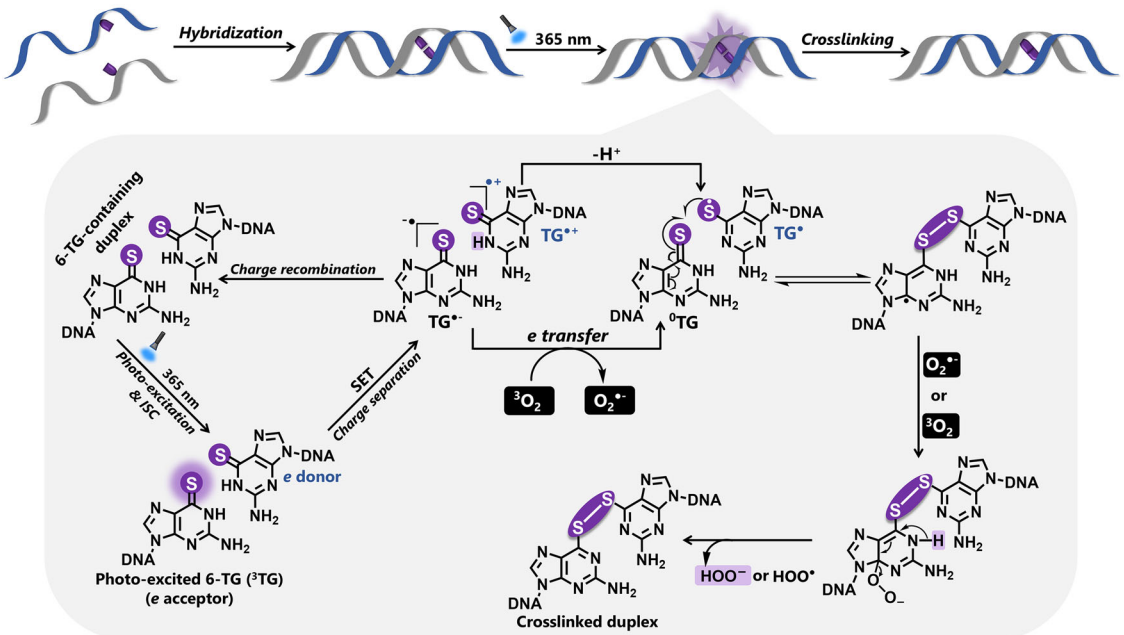

Fig. 8 | Postulated reaction mechanism of photoinduced disulfide crosslink formation in the designed TG-containing oligo DNA duplex. ^{3}TG induces charge separation via a single electron transfer (SET) process. Under air-saturated conditions, $^3O_2$ drives the formation of disulfide crosslink through reactions involving $O_2^{\bullet-}$ and $TG^{\bullet}$ intermediate.

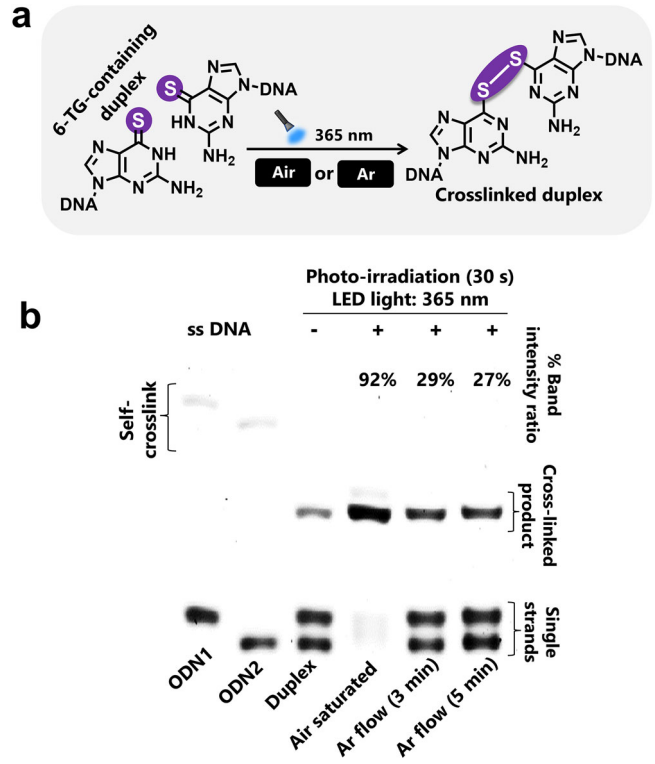

Fig. 9 | Effect of O_2 on photoinduced disulfide crosslinking efficiency. a Schematic illustration of crosslinking reaction under argon (Ar) atmosphere to evaluate the influence of O_2. **b** PAGE analysis for reaction efficiency under Ar atmosphere versus air-saturated conditions. ODN strands (10 μM each) were prepared in phosphate buffer (20 mM, pH 7.0) containing NaCl (100 mM); photoreaction was then performed using 365 nm LED light (UV light intensity: 3.0 W/m²) for 30 s at 0 °C in an open tube (air-saturated) or in a sealed tube flushed with Ar for 3 or 5 min, followed by irradiation under Ar flow. PAGE analysis condition: 16% acrylamide, 20% formamide, SYBR™ Gold staining, and ChemiDoc MP imaging system. Quantitative analysis of the crosslinked product (% band intensity) showed a marked decrease in reaction efficiency under Ar conditions compared to air-saturated conditions. The crosslinking yield was calculated from the intensity of the crosslinked product band over the sum of the product and remaining single-stranded ODNs.

As a further attempt, we sought to identify the predominant ROS involved in the photosensitization process by using various scavengers and assessing their impact on the photochemical reaction (Fig. S10a). Photoirradiation experiments were conducted in the presence of mannitol (a hydroxyl radical $^{\bullet}OH$ quencher)[73,74], superoxide dismutase (SOD, an $O_2^{\bullet-}$ scavenger)[75,76], and sodium azide (a $^1O_2$ quencher)[77], at varying concentrations, with reaction outcomes analyzed via PAGE. However, even at high scavenger concentrations, no significant modulation in reaction efficiency was observed (Fig. S10b, S10c, S10d). The quenching of these species did not noticeably affect reaction yield, suggesting that none play a direct role in driving crosslink formation. This finding supports our proposed mechanism, in which $O_2^{\bullet-}$ is a byproduct of electron transfer to $^3O_2$ rather than a direct contributor to the crosslinking reaction.

As an alternative approach, we attempted to detect photogenerated $O_2^{\bullet-}$ in the reaction system using nitro blue tetrazolium chloride (NBT) as a detection probe. NBT, a yellow, water-soluble compound, specifically reacts with $O_2^{\bullet-}$ to form formazan, a purple, water-insoluble product with a characteristic absorption in the wavelength range of 500–600 nm, detectable via UV–Vis spectroscopy (Fig. 10a)[104,105]. To investigate $O_2^{\bullet-}$ production, the oligo DNA duplex was irradiated with 365 nm UV light in the presence of NBT. Since 10 s of irradiation was sufficient for efficient crosslinking, we performed $O_2^{\bullet-}$ detection at 10 s and 1.0 min for comparison. The formation of formazan, indicating $O_2^{\bullet-}$ generation, was monitored via UV–Vis spectroscopy. As a negative control, a buffer solution containing only NBT, without oligo DNA, was irradiated under identical conditions. The UV–Vis spectra showed no absorption in the wavelength range of 500–600 nm (Fig. 10b), confirming the absence of formazan formation. In contrast, the duplex irradiated for 10 s exhibited a strong absorption band in this range (Fig. 10c), confirming $O_2^{\bullet-}$ generation.

Interestingly, when a single-stranded oligo DNA was irradiated for 10 s, no corresponding formazan absorption was observed (Fig. 10d), suggesting that $O_2^{\bullet-}$ was not produced under these conditions. However, after 1.0 min of irradiation, a weak absorption band appeared, indicating delayed $O_2^{\bullet-}$ generation compared with the duplex (Fig. 10d). These findings suggest that the duplex structure facilitates $O_2^{\bullet-}$ production by enabling faster electron transfer kinetics than the single-stranded oligo DNA. The rigid duplex conformation, along with the proximity effect provided by the hybridized structure, aligns the electron donor (^{0}TG) and acceptor (^{3}TG) in a favorable geometry for rapid SET (Fig. 10f). Consequently, under short irradiation (10 s), charge separation generates $TG^{\bullet-}$ and $TG^{\bullet+}$ species, followed by electron transfer to $^3O_2$, enabling $O_2^{\bullet-}$ detection. In contrast, the single-stranded ODN lacks these structural constraints (Fig. 10g), reducing the likelihood of favorable alignment between the reactive components and making the SET step less efficient. Consequently, the reaction exhibits slower kinetics, requiring longer irradiation times for detectable $O_2^{\bullet-}$ generation. This was confirmed by irradiating the single strand for 1 h, which led to more pronounced $O_2^{\bullet-}$ production in a concentration-dependent manner (Fig. S11).

We have confirmed that crosslinking terminates $O_2^{\bullet-}$ generation. This was demonstrated by irradiating a solution containing the crosslinked product in the presence of NBT, where no absorption band was observed in the 500–600 nm range (Fig. 10e), indicating the absence of detectable $O_2^{\bullet-}$. Collectively, these results underscore the critical role of the DNA duplex structure in facilitating rapid electron transfer and efficient $O_2^{\bullet-}$ generation. In the duplex system, $O_2^{\bullet-}$ is generated swiftly through electron transfer to $^3O_2$. However, once crosslinking occurs and no free TG is available for further electron transfer, $O_2^{\bullet-}$ generation is suppressed, aligning with our proposed reaction mechanism.

Our mechanism suggests that the neutral thiyl radical ($TG^{\bullet}$) forms as an intermediate during the crosslinking reaction through the oxidation and proton loss of $TG^{\bullet+}$. Based on this hypothesis, we anticipated that chemical reduction could restore oxidized $TG^{\bullet}$ back to ^{0}TG, thereby propagating $O_2^{\bullet-}$ generation (Fig. 11a). This hypothesis is supported by a previous study[100], which reported that monitoring 6-TG monomer/UVA-induced photosensitization in the presence of GSH induces $O_2^{\bullet-}$ oxidation–GSH reduction cycles, with the thiyl radical as an intermediate. To test this hypothesis, we irradiated a TG-containing single strand in the presence of GSH as a reducing agent and monitored $O_2^{\bullet-}$ generation using the NBT assay. The solution containing GSH exhibited a significantly higher absorption intensity corresponding to the formazan compound compared to the solution without GSH (Figs. 11b and S12a), indicating enhanced $O_2^{\bullet-}$ generation. This increase was further confirmed visually, as the GSH-containing solution displayed a more intense purple color (Figs. 11c and S12b), indicative of greater formazan formation. These results strongly support the formation of the thiyl radical as a key intermediate in the photosensitization process. Reduction of $TG^{\bullet}$ by GSH sustains photoinduced $O_2^{\bullet-}$ generation (Path A, Fig. 11a). However, after prolonged photo-irradiation, when GSH is fully oxidized to GSSG, the thiyl radical is expected to rapidly react with $^3O_2$ (Path B, Fig. 11a)[100], leading to the formation of various oxidation products[95–97].

Our proposed mechanism is further supported by the likely formation of hydrogen peroxide (H_2O_2) as a secondary byproduct. This H_2O_2 could originate from species generated during the photoinduced reaction, either through protonation of the hydroperoxide anion (HOO^-) or recombination of a hydroperoxyl radical ($HOO^{\bullet}$) with $O_2^{\bullet-}$. To confirm its presence, we used the OxiVision™ Green sensor, an H_2O_2-selective fluorescent probe. A strong fluorescence response was observed when the probe was incubated with a 10 s photoirradiated duplex solution compared to the nonirradiated control (Fig. S13), confirming H_2O_2 generation upon photoirradiation.

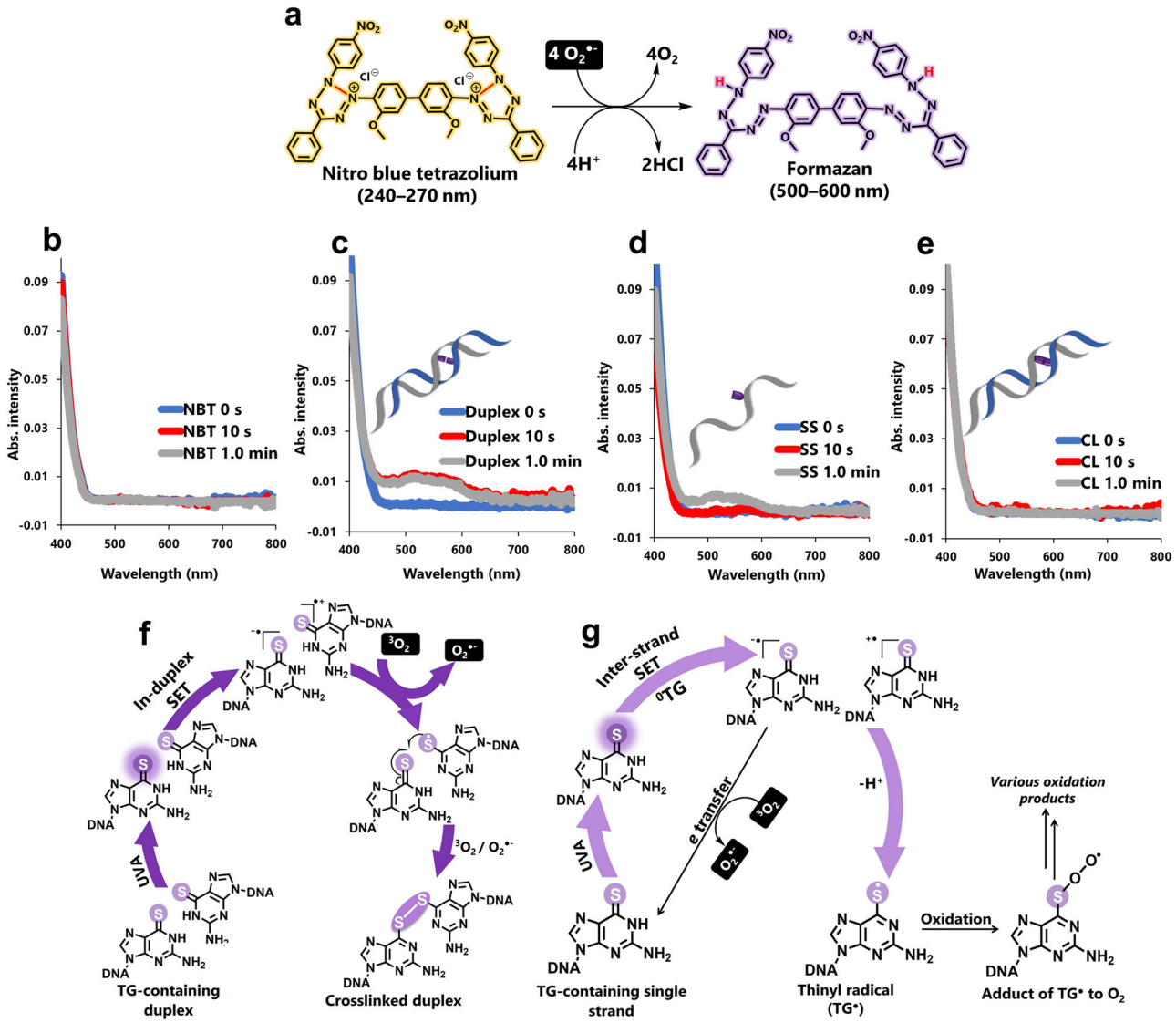

Fig. 10 | Photogeneration of superoxide radical ($O_2^{\bullet-}$) and electron-transfer behavior in TG-containing oligo-DNA systems. a–e: Detection of the photo-generated $O_2^{\bullet-}$ using nitro blue tetrazolium (NBT). **a** Schematic of $O_2^{\bullet-}$ detection using NBT as a detection probe to form the UV-detectable formazan compound. UV–Vis spectra showing the absorption intensity at approximately 500–600 nm (corresponding to formazan) for different samples: **b** negative control (buffer solution containing NBT without ODN), **c** duplex solution, **d** single-stranded ODN, and **e** crosslinked product solution (10 s preirradiated duplex). All samples were photoirradiated in the presence of NBT. Conditions: single-stranded ODN, duplex, or CL product (40 μM, 4.0 μL) was irradiated with NBT (600 μM) in 20 mM phosphate buffer (pH 7.0, containing 100 mM NaCl) at 0 °C using a 365 nm UV LED (UV light intensity: 34.1 W/m^2) for 10 s or 1 min. Formazan formation was analyzed by UV–Vis (400–800 nm) spectroscopy after dilution with DMSO. **f, g: SET kinetics in duplex vs. Single-stranded oligo-DNA systems**. **f** In-duplex SET: The duplex structure facilitates faster $O_2^{\bullet-}$ generation by promoting efficient SET kinetics through a proximity effect, which aligns the donor (^{0}TG) and acceptor (^{3}TG) in a favorable geometry. **g** Interstrand SET: The single-stranded system exhibits inefficient SET kinetics, leading to slower electron transfer and undetectable $O_2^{\bullet-}$ levels under short photoirradiation time.

Taken together, these findings provide strong mechanistic support for our proposed reaction pathway. The initiation of the reaction via charge separation and SET is evidenced by the accelerated $O_2^{\bullet-}$ generation in the duplex system. Moreover, we confirmed that $^3O_2$ plays a crucial role in facilitating the electron transfer step, resulting in $O_2^{\bullet-}$ generation, which is efficiently detected in our system as an electron transfer product rather than as a direct driving force of the reaction. Additionally, our results indicate that the reaction proceeds via a thiyl radical intermediate, which enables interstrand crosslinking.

Impact of TGs orientation on photoinduced crosslinking efficiency

Having elucidated the underlying photoinduced crosslinking reaction mechanism, we next sought to rationalize the lack of reactivity observed in the opposite orientation upon photoirradiation (Fig. 6g, i). To this end, we compared the efficiency of $O_2^{\bullet-}$ generation in the ODN2–ODN3 duplex (opposite orientation) using the NBT method with that in the ODN1–ODN2 duplex (original design) as a positive control. While the original design generated $O_2^{\bullet-}$ efficiently within 10 s of irradiation (Fig. 10c), no detectable $O_2^{\bullet-}$ was observed for the opposite orientation under the same conditions (Fig. 12a). Detectable levels appeared only after 1.0 min of irradiation, indicating that the opposite orientation exhibited a notable delay in $O_2^{\bullet-}$ generation. These results are consistent with the lack of crosslinking reactivity in the opposite orientation.

As noted earlier, structural analysis of the two duplex designs using molecular modeling revealed key differences in the orientation and angular alignment of the TG residues. When viewed from the same angle, a striking difference in their relative positioning was apparent. In the original design

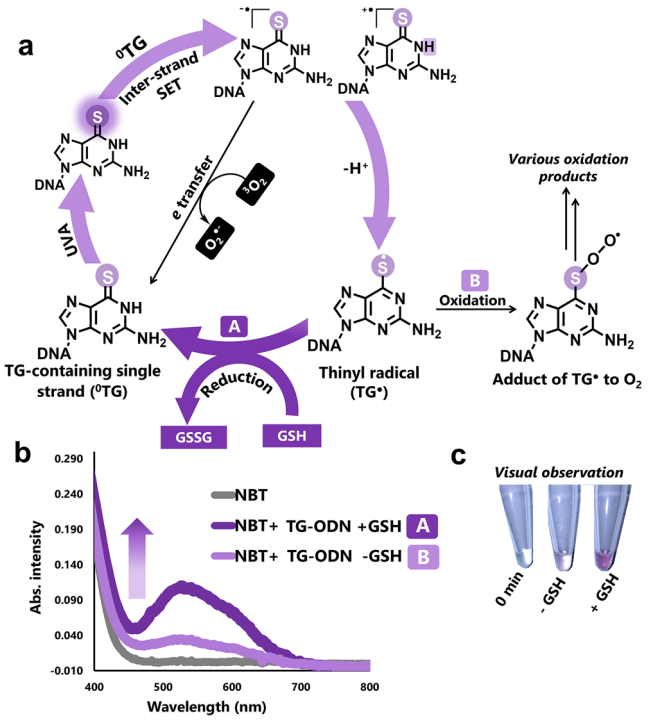

Fig. 11 | Effect of GSH on the restoration of thiyl radicals and propagation of $O_2^{\bullet-}$ generation. a Scheme showing $O_2^{\bullet-}$ generation and formation of thiyl radicals in TG-containing single strand. Path **A** (+GSH): reduces TG• back to ^{0}TG, promoting continuous generation of photoinduced $O_2^{\bullet-}$. Path **B** (−GSH): in the absence of GSH, TG• undergoes oxidation, leading to the gradual loss of $O_2^{\bullet-}$ generation over time. **b** NBT assay results: UV–Vis absorption spectra showing the absorption band intensity corresponding to the formazan compound in TG-containing single-strand oligo DNA irradiated with and without GSH. **c** Visual observation result showing more intense purple color, indicative of formazan formation, in the solution with GSH compared to the solution without GSH. Conditions: Single-stranded ODN (60 μM, 4.0 μL) was irradiated with 600 μM NBT in 20 mM phosphate buffer (pH 7.0, 100 mM NaCl) with or without 300 μM GSH at 0 °C using a 365 nm UV LED (UV light intensity: 3.0 W/m²) for 1 h. Formazan formation was analyzed by UV-Vis (400–800 nm) after dilution with DMSO.

(ODN1–ODN2 duplex), the TG residues were oriented away from each other rather than directly stacked on top, resulting in larger spatial separation. This observation is consistent with the longer interatomic distances (N1–N1 = 4.76 Å, C2–C2 = 5.76 Å), which suggests reduced overlap of the reactive groups (Fig. S14a, S14b). In contrast, the opposite orientation (ODN3–ODN2 duplex) caused the TG residues to be more directly stacked, leading to a closer spatial approach. This is consistent with the shorter interatomic distances (N1–N1 = 3.80 Å, C2–C2 = 3.69 Å), which reflect partial overlapping of the residues (Fig. S14a, S14b).

These structural differences align well with the experimental results of $O_2^{\bullet-}$ generation and can be rationalized within the proposed reaction mechanism. In the original design, the TG residues point in directions that maintain sufficient spatial separation for charge-separated species to persist long enough for TG$^{\bullet-}$ to transfer an electron to O_2, efficiently producing $O_2^{\bullet-}$. In contrast, the opposite orientation (ODN3–ODN2 duplex) has partial overlapping between TG residues, which facilitates rapid charge recombination (Fig. 12b) that shortens the lifetime of TG$^{\bullet-}$. This limits its ability to transfer an electron to O_2 and thereby results in slower $O_2^{\bullet-}$ generation.

Collectively, by taking all structural analyses into account, these findings demonstrate that the orientation and degree of overlap of TG residues within a DNA duplex dictate photoinduced crosslinking. In the original design, the pre-organized duplex structure minimizes the angular adjustments required for crosslinking, while the smaller overlap between TG residues enables effective electron transfer to O_2, leading to efficient $O_2^{\bullet-}$ generation and disulfide crosslinking. In the opposite orientation, the poorly pre-organized duplex structure requires major conformational adjustments, and the closely stacked TG residues accelerate charge recombination, which slows electron transfer to O_2 and delays $O_2^{\bullet-}$ formation. This ultimately reduces the photoinduced reactivity toward crosslinking.

Repetitive reversibility of crosslinking reaction

We next examined the ability of our oligo DNA duplex design to undergo multiple cycles of crosslink formation and cleavage under controlled conditions without significant loss of functionality or structural integrity. This property is essential for applications requiring reversible crosslinking for dynamic control, such as stimuli-responsive materials[59], drug delivery systems[66,106], and biochemical studies[107,108]. Maintaining the crosslinking performance over multiple cycles would enable repeated switching between the crosslinked and non-crosslinked states, making the system suitable for such applications. To assess this, we tested the reversibility under chemical oxidation using I_2 and reduction using DTT (Fig. 13a). PAGE analysis confirmed that excess I_2 efficiently induced crosslink formation, whereas excess DTT cleaved the disulfide bonds (Fig. 13b). This cycle was repeated effectively for three iterations, demonstrating consistent disulfide bond formation and cleavage without loss of efficiency.

We also tested the reversibility of crosslinking under photo-oxidation and DTT reduction conditions (Fig. 13c). DTT temporarily inhibits crosslink generation by cleaving disulfide bonds; however, prolonged photoirradiation depletes DTT, enabling high-yield crosslink formation. The minimum DTT concentration required for effective cleavage of the photoinduced crosslink product was 100 μM (Fig. S15a). Adding 2,2′-dipyridyl disulfide (Py–SS–Py) as a disulfide trapping reagent enabled the sequestration of DTT, permitting crosslinking to resume under extended photoirradiation (up to 10 min) (Fig. S15b). Over time, thiol-disulfide exchange mediated by Py–SS–Py oxidized DTT, reducing its cleavage efficiency and allowing high-yield crosslinking. Under these conditions, photoinduced crosslinking remained effective for up to three cycles (Fig. 13d). After the second crosslinking step, a negligible yield of a side crosslink product was observed; however, the intended disulfide crosslink remained the dominant product throughout the cycles. To evaluate the biological relevance of this system, we examined the stability of disulfide-crosslinked duplexes in cell lysates. The disulfide crosslinks were rapidly cleaved within 1 min upon incubation in the lysate (Fig. S16), demonstrating that this system responds efficiently to intracellular reducing environments under physiologically relevant conditions. This reversible property could enable applications in structural dynamics studies as well as in targeted release within biochemical systems[66,109].

To expand this crosslinking strategy beyond simple DNA duplexes, we examined its applicability to structurally diverse nucleic acid systems. A 72-mer linear DNA strand was designed with TG residues incorporated into the complementary regions near the 5′ and 3′ ends, along with two poly(T)$_{14}$ flexible spacers to facilitate strand folding (Fig. S17a). This design brings the TG residues near the 5′ and 3′ ends into proximity, enabling intramolecular disulfide bond formation under oxidative conditions and resulting in a disulfide-crosslinked stem-loop structure (Fig. S17a). Both chemical oxidation and photoirradiation conditions efficiently promoted crosslinking, and subsequent treatment with reducing agents restored the linear form (Fig. S17b, S17c). Reversibility was confirmed through repeated redox cycling: sequential I_2-mediated oxidation and DTT reduction allowed multiple cycles of bond formation and cleavage (Fig. S17b), whereas photoirradiation–DTT cycles showed reduced efficiency after the first cycle, likely due to partial hydrolysis of TG residues (Fig. S17c). This reversible redox-responsive switching offers promising applications because disulfide cleavage can be precisely triggered by the intracellular environment to restore the linear construct and enable controlled intracellular release. Importantly, these results demonstrate that disulfide-based crosslinking can be applied beyond simple duplexes to more structurally complex nucleic acid architectures.

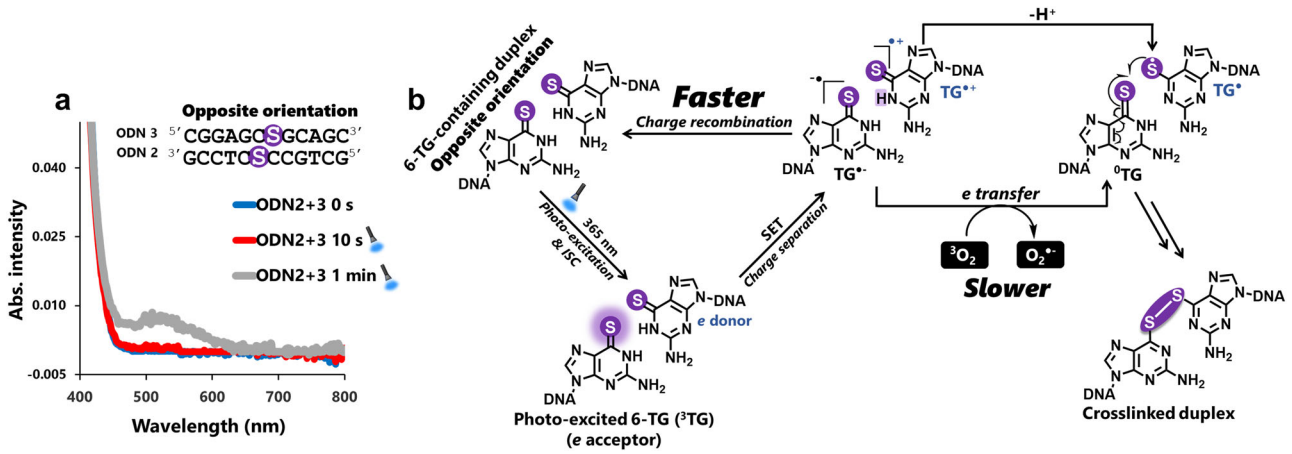

Fig. 12 | Impact of TGs orientation on photoinduced crosslinking efficiency. a $O_2^{\bullet-}$ generation in the ODN2–ODN3 duplex (opposite orientation) measured by the NBT assay under photoirradiation. Conditions: duplex (40 μM, 4.0 μL) was irradiated with NBT (600 μM) in 20 mM phosphate buffer (pH 7.0, containing 100 mM NaCl) at 0 °C using a 365 nm UV LED (UV light intensity: 34.1 W/m^2) for 10 s or 1 min. Formazan formation was analyzed by UV–Vis (400–800 nm) spectroscopy after dilution with DMSO. **b** Schematic illustrating how the opposite orientation of TG residues accelerates charge recombination, shortens the lifetime of $TG^{\bullet-}$, and reduces electron transfer efficiency to O_2.

Conclusions

Herein, we successfully demonstrated that incorporating non-complementary 2′-deoxythioguanines within an oligo DNA duplex enables efficient interstrand disulfide crosslinking through proximity-driven reactions under various oxidation conditions, without significantly distorting the B-DNA helix. This design facilitated rapid crosslinking within 1 min under chemical oxidation, achieving a nearly quantitative yield (95%), and introduced a novel photoinduced reaction that afforded disulfide crosslink formation within 10 s of 365 nm UV irradiation with 93% yield. Formation of the intended disulfide-crosslinked product was confirmed through multiple experiments, including its susceptibility to cleavage under reducing conditions and enzymatic digestion, which identified disulfide-crosslinked guanosine nucleosides as the exclusive product, indicating a clean reaction profile. The crosslinked duplexes exhibited significantly enhanced thermal stability ($T_m > 80$ °C) compared with the noncrosslinked duplex (47 °C), confirming successful covalent strand linkage formation.

The designed proximity and precise positioning of the reactive thiocarbonyl groups in the 2′-deoxythioguanosine-incorporated duplex structure were critical for achieving efficient disulfide crosslinking. Additionally, it was demonstrated that the orientation of TG residues within a DNA duplex dictates both the efficiency and selectivity of crosslink formation. In the ODN1–ODN2 design, the TG in ODN1 was positioned in a 5′-offset manner relative to the TG in ODN2, which yielded a pre-organized duplex structure that required only minor conformational changes and small angular adjustments, thereby minimizing the activation energy for efficient crosslinking. In the ODN2–ODN3 design, the TG in ODN3 was positioned in a 3′-offset manner relative to the TG in ODN2, which produced a poorly pre-organized duplex that required major conformational adjustments and increased the activation energy. This, in turn, slowed the disulfide crosslinking reaction and promoted competing reactions under chemical oxidation. The structure of the resulting DTT-resistant product and the mechanistic details of its formation are currently being elucidated.

Mechanistic investigations of photoinduced disulfide crosslink formation revealed that (1) the reaction is initiated by SET followed by charge separation, where photoexcited ^{3}TG acts as an electron acceptor, accepting an electron from ^{0}TG to generate $TG^{\bullet-}$ and $TG^{\bullet+}$ radicals; (2) molecular oxygen ($^3O_2$) plays a crucial role in the electron transfer step, driving the reaction toward disulfide bond formation; (3) $O_2^{\bullet-}$ is produced as a byproduct of electron transfer to $^3O_2$; and (4) $TG^{\bullet}$ is a key intermediate in the process.

We further confirmed that $O_2^{\bullet-}$ is generated upon photoirradiation with distinct kinetics: duplex system exhibits faster $O_2^{\bullet-}$ generation, but once the disulfide crosslink forms and 6-TG is depleted, further SET and electron transfer to $^3O_2$ are suppressed. In single-stranded 6-TG system, $O_2^{\bullet-}$ generation occurs more slowly and is dependent on 6-TG concentration and irradiation time. Over time, $O_2^{\bullet-}$ generation diminishes as $TG^{\bullet}$ rapidly reacts with $^3O_2$, forming various oxidation products. However, GSH-mediated reduction of $TG^{\bullet}$ regenerates 6-TG, sustaining further $O_2^{\bullet-}$ production.

Additionally, we demonstrated that our duplex design permits reversible crosslinking, allowing multiple cycles of crosslink formation and cleavage under oxidation–reduction conditions. Furthermore, this redox-responsive switching between crosslinked and noncrosslinked states can be extended to more structurally complex nucleic acid constructs. Such reversible redox responsiveness holds promise for developing dynamic DNA-based systems for nanotechnology, drug delivery, and biotechnological applications.

The design principles established here, together with the insights from molecular modeling and mechanistic elucidation of the reaction mechanism, provide a valuable foundation for the rational design of nucleic acid crosslinking strategies. Beyond the validation of proximity-driven crosslinking and photoinduced reactivity, these findings highlight the potential of thioguanine-mediated chemistry as a versatile platform for dynamic and reversible covalent modifications of nucleic acids. Such advances are expected to broaden the scope of nucleic acid chemistry and facilitate future applications of chemically and photoinduced crosslinking.

Methods

Synthesis of 2′-deoxythioguanosine phosphoramidite and its incorporation into oligo DNA

First, 2′-deoxyguanosine was protected with *tert*-butyldimethylsilyl (TBDMS) groups to yield **compound 1**. Compound 1 was then reacted with 2-mesitylenesulfonyl chloride to activate the 6-position of guanine, forming a sulfonate ester intermediate. This intermediate was subsequently treated with 2-ethylhexyl 3-mercaptopropionate in the presence of N-methylpyrrolidine to yield compound 2. Next, the 2-amino group of **compound 2** was protected with phenoxyacetyl chloride to yield **compound 3**. The TBDMS groups were then removed using tetrabutylammonium fluoride (TBAF), resulting in the corresponding diol product, **compound 4**. The 5′-hydroxyl group of compound 4 was selectively protected with 4,4-dimethoxytrityl (DMTr) chloride in pyridine to form **compound 5**. The phosphoramidite derivative of compound 5 was synthesized using 2-cyanoethyl-*N*,*N*-diisopropylchlorophosphoramidite, affording **compound 6** (Scheme S1). Compound 6 was successfully

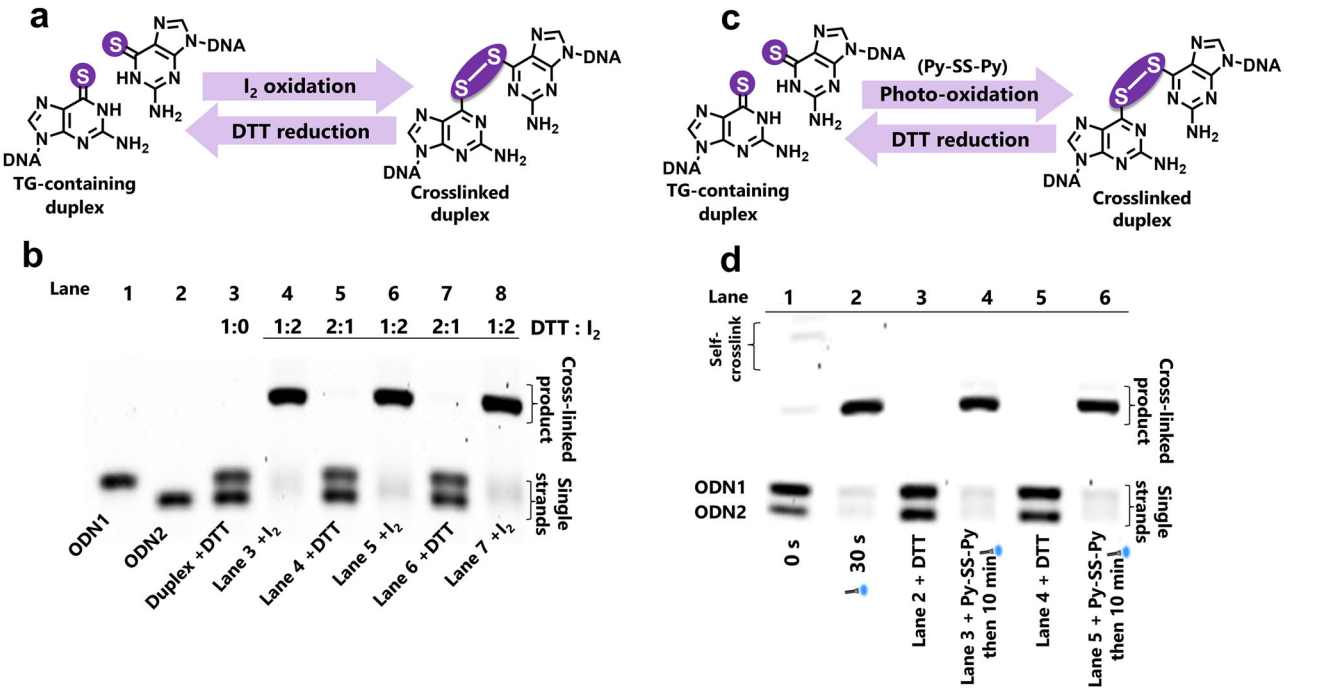

Fig. 13 | Repetitive reversibility of crosslinking reactions: Multiple cycles of disulfide bond formation and cleavage analyzed by PAGE. a, **b** Chemical oxidation (I_2) and reduction with DTT. Conditions: ODN strands (10 μM each), phosphate buffer pH 7.0 (20 mM), NaCl (100 mM), DTT (100 μM), I_2 (200 μM), incubated at 10 °C (lane 4), then maintaining DTT:I_2 ratios of 2:1 for cleavage and 1:2 for crosslinking (lanes 5–8). **c**, **d** Photo-oxidation in the presence of Py–SS–Py followed by DTT reduction. Conditions: ODN strands (10 μM each), phosphate buffer pH 7.0 (20 mM), NaCl (100 mM), Py–SS–Py (100 μM), DTT (100 μM), 365 nm LED light (UV light intensity: 3.0 W/m²) for 10 min at 0 °C.

incorporated into oligo DNA through a standard solid-phase synthesis approach using an automated DNA synthesizer (Scheme S2) and purified by HPLC to yield the intended ODN sequences (see SI).

MALDI–TOF MS measurement

Lyophilized ODN samples obtained after HPLC purification were dissolved in H_2O for MALDI–TOF MS analysis. The matrix was prepared by mixing di-ammonium hydrogen citrate (5 mg/50 μL, in H_2O) with 3-hydroxypicolinic acid (25 mg/500 μL, in 1:1 H_2O/CH_3CN, v/v). A 1 μL aliquot of the matrix solution was first spotted onto the MALDI sample plate, followed by 1 μL of the ODN sample solution. After drying at room temperature, the samples were analyzed by MALDI–TOF mass spectrometry.

Disulfide crosslinking under iodine reaction conditions (PAGE analysis)

A duplex formed from the complementary sequences ODN1 and ODN2 (10 μM each) was incubated with iodine (100 μM, prepared in DMSO) in a phosphate buffer solution (20 mM, pH 7.0) containing NaCl (100 mM) at 10 °C. The total reaction volume was 4.0 μL. The reaction mixture was quenched by adding a loading buffer containing 10 mM EDTA in 80% formamide and analyzed using denaturing 16% polyacrylamide, 20% formamide gel electrophoresis. The gel image was visualized using SYBR™ Gold stain.

Preparative disulfide crosslink under iodine reaction conditions (large scale)

A large-scale crosslinking reaction under iodine conditions was performed as described above, with the oligo DNA amount increased to 500 pmol. The reaction solution was then desalted using Sep-Pak® C18 Plus short cartridge (Waters™) and purified using an illustra™ NAP™-5 column (Cytiva). The collected fraction containing the crosslinked product was dried by lyophilization.

Photoinduced disulfide crosslinking reaction (PAGE analysis)

Complementary strands (10 μM each) were prepared in phosphate buffer (20 mM, pH 7.0) containing 100 mM NaCl and irradiated at 0 °C using a 365 nm LED light source. The total volume of the irradiated solution was 4.0 μL. The reaction mixture was quenched by adding a loading buffer containing 10 mM EDTA in 80% formamide and analyzed using denaturing 16% polyacrylamide and 20% formamide gel electrophoresis. The gel image was visualized using SYBR™ Gold stain.

Preparative disulfide crosslinking under photoirradiation conditions (large scale)

The photoreaction was performed as described above using a total oligo concentration of 10 μM in a 4.0 μL reaction volume and repeated 12 times to achieve a total oligo amount of 500 pmol. The photoirradiated reaction solutions were combined, desalted using Sep-Pak® C18 Plus short cartridge (Waters™), and lyophilized.

Characterization of self-crosslinked products

Self-crosslinked products were isolated by HPLC under the following conditions: NACALAI TESQUE, COSMOSIL, 5C18-MS-II packed column (10 ID × 250 mm), gradient system: (A) 0.1 M TEAA buffer, (B) 5%–30% acetonitrile over 20 min followed by a linear gradient to 100% over 20–30 min, column temperature: 35 °C, flow rate of 1 mL/min, and detection using a UV detector at 254 nm. HPLC-purified self-crosslinked products were analyzed by PAGE after DTT treatment. ODNs (10 μM) in phosphate buffer (20 mM, pH 7.0) containing NaCl (100 mM) were incubated with DTT (200 μM) at 10 °C for 30 min, and samples were subsequently analyzed by denaturing PAGE (16% acrylamide, 20% formamide) and visualized by SYBR™ Gold staining.

HPLC quantification of crosslinking yield

Crosslinking reactions were performed on a 500 pmol scale by using ODN1 and ODN2 under the conditions described above. Reaction yields were

quantified by HPLC with single-stranded ODNs and duplex standards used as references for peak assignment and normalization. The crosslinking yield was calculated as the percentage of the normalized product peak area relative to the sum of all normalized peak areas, where each HPLC peak area was divided by the corresponding molar extinction coefficient at 260 nm ($\varepsilon = 260$ nm). HPLC Conditions: NACALAI TESQUE, COSMOSIL, 5C18-MS-II packed column (10 ID × 250 mm), gradient system was conducted at a column temperature of 45 °C, flow rate of 1 mL/min, and detection using a UV detector at 254 nm: (A) 0.1 M TEAA buffer and (B) acetonitrile at 5%–30% over 20 min followed by a linear gradient to 100% over 20–30 min.

Enzymatic digestion experiment of crosslinked products and HPLC analysis

To the lyophilized reaction mixture containing 500 pmol of crosslinked products, 17.0 μL of distilled, sterilized H_2O was added, followed by 2.0 μL of 10X nucleoside digestion mix reaction buffer and 1.0 μL of nucleoside digestion mix (New England Biolabs). The reaction mixture was incubated at 37 °C for 3 h. Samples were analyzed by HPLC under the following conditions: COSMOSIL 5C18-AR-II Packed Column (4.6 × 250 mm), gradient system with (A) 50 mM NH_4COOH and (B) acetonitrile, 0%–40% (B) over 20 min, followed by a linear gradient to 100% (B) over 20–30 min, column temperature of 35 °C and flow rate of 1 mL/min. The chromatograms show retention time (X-axis) from 0–25 min, and the peaks correspond to detector response (intensity, Y-axis) monitored at 254 nm, with an approximate signal range of 0–450,000 μV. A new peak with a longer retention time appeared in the HPLC profile. The corresponding fractions were separated, lyophilized, and analyzed by ESI-MS. The observed mass spectrum data were as follows: ESI-HRMS (*m/z*): $[M + H]^+$ calcd for disulfide crosslinked guanosine adduct $[C_{20}H_{24}N_{10}O_6S_2]^+$: 565.1394, found: 565.1381.

Melting temperature (T_m) measurements

For melting temperature (T_m) measurements, a 100 μL solution of duplex (2.0 μM) in phosphate buffer (20 mM, pH 7.0) containing NaCl (100 mM) was transferred to a micro quartz cell with a 1-cm path length. The melting temperature was measured by UV absorption at 260 nm from 0 °C to 90 °C at a rate of 1.0 °C/min. Each sample was measured three times, and the results were averaged to obtain the final value. The melting temperature was measured using a V-730 (JASCO Corporation) spectrophotometer equipped with a temperature controller.

CD spectrum measurements

A 100 μL solution of duplex (4.0 μM) in phosphate buffer (20 mM, pH 7.0) containing NaCl (100 mM) was transferred to a microquartz cell with a 1-cm path length. The CD spectra were analyzed at 25 °C over a wavelength range of 210–350 nm using a J-720WI (JASCO Corporation) spectropolarimeter equipped with a temperature controller.

Disulfide crosslinking in TG-modified duplexes: sequence and orientation dependency

Chemical oxidation conditions: Complementary ODN strands (10 μM each) were prepared in phosphate buffer (20 mM, pH 7.0) containing NaCl (100 mM) were incubated with DTT (100 μM) at 10 °C for 30 min to reduce self-crosslinked species. Crosslinking was then induced by treatment with I_2 (200 μM) at 10 °C for 1 h. The resulting crosslinked products were subsequently incubated with DTT (200 μM) at 10 °C for 30 min prior to analysis.
Photoinduced crosslinking conditions: Duplexes (10 μM) were prepared in phosphate buffer (20 mM, pH 7.0) containing NaCl (100 mM) and irradiated with 365 nm LED light (UV intensity: 3.0 W/m^2) for 30 s at 0 °C. The resulting crosslinked products were then incubated with DTT (200 μM) at 10 °C for 30 min prior to analysis.
PAGE analysis: Samples were analyzed by denaturing PAGE (16% acrylamide, 20% formamide) and visualized with SYBR™ Gold staining.

Testing photoinduced crosslinking under argon (Ar) atmosphere

The photoreaction solution was prepared as described above, and the experiment was conducted by sealing the reaction tube with a plastic septum and parafilm and then flushing it with argon gas through a syringe to remove air. The sealed reaction tube was irradiated with 365-nm light under an argon flow. The reaction mixture was then quenched by adding a loading buffer (containing 10 mM EDTA in 80% formamide) and analyzed by denaturing 16% polyacrylamide and 20% formamide gel electrophoresis. SYBR™ Gold staining was used to visualize the gel image.

Detection of photogenerated superoxide radicals using the NBT method

For the detection of photogenerated superoxide radicals using the NBT method, solutions (4.0 μL) of single-stranded ODN, duplex, or a solution containing the CL product (10-s preirradiated duplex) at 40 μM were irradiated with 600 μM NBT in a 20 mM phosphate buffer (pH 7.0) containing 100 mM NaCl at 0 °C using a 365 nm UV LED light source (UV light intensity: 34.1 W/m^2) for 10 s and 1.0 min. After photoirradiation, the solutions were diluted with DMSO to dissolve the formed formazan compound and analyzed using a UV–Vis spectrophotometer over a wavelength range of 400–800 nm.

Testing the effect of GSH on the propagation of superoxide radical generation using NBT method

To test the effect of GSH on the propagation of superoxide radical generation using the NBT method, solutions (4.0 μL) of single-stranded ODN (60 μM) were irradiated with 600 μM NBT in 20 mM phosphate buffer (pH 7.0) containing 100 mM NaCl and 300 μM GSH at 0 °C using a 365 nm UV LED light source (UV light intensity 2.96 W/m^2) for 1.0 h. After photoirradiation, the solutions were diluted with DMSO to dissolve the formed formazan compound and analyzed using a UV–Vis spectrophotometer over a wavelength range of 400–800 nm. The same experiment was performed without including GSH in the photoreaction mixture.

Detection of hydrogen peroxide generation in the photoreaction mixture

A solution (4.0 μL) of duplex (40 μM) in a 20 mM phosphate buffer (pH 7.0) containing 100 mM NaCl was irradiated at 0 °C using a 365 nm UV LED light source for 10 s (UV light intensity: 34.1 W/m^2), then incubated with 10 μM OxiVision Green™ hydrogen peroxide sensor at room temperature for 45.0 min. Fluorescence emission spectra were recorded using a fluorescence spectrometer ($\lambda_{ex} = 490$ nm) at 25 °C. The same experiment was performed using a duplex solution without photoirradiation and a photoirradiated blank solution in the absence of duplex.

Repetitive reversibility of crosslinking reaction

Chemical oxidation (I_2) and reduction (DTT): For I_2-mediated oxidation and DTT reduction, a 100 μM I_2 crosslinking reaction solution was prepared as previously described and incubated with 200 μM DTT at 10 °C. The crosslinked product was then recovered by adding 200 μM I_2 to the same solution and incubating at 10 °C. This cycle of crosslink formation and cleavage was repeated thrice, maintaining a DTT:I_2 concentration ratio of 2:1 for cleavage and 1:2 for crosslinking. After each step, the reaction solutions were analyzed by denaturing 16% polyacrylamide, 20% formamide gel electrophoresis, and the gel image was visualized using SYBR™ Gold stain.
Photo-oxidation and DTT reduction: For the photo-oxidation and DTT reduction experiments, a solution of the photoinduced crosslink product was incubated with 100 μM DTT, followed by the addition of 100 μM 2,2′-dipyridyl disulfide (Py–SS–Py). The solution was then photoirradiated using a 365 nm UV LED for 10.0 min at 0 °C (UV light intensity 3.0 W/m^2). This process was repeated three times, and all reaction solutions were analyzed using denaturing 16% polyacrylamide, 20% formamide gel electrophoresis, with visualization using SYBR™ Gold stain.

Stability of the crosslinked products in cell lysate

Reaction mixtures containing HPLC-purified I_2-induced and photoinduced crosslinked products (2.5 μM) in phosphate buffer (20 mM, pH 7.0) were incubated with HeLa whole-cell lysate (0.125 μg/μL; Santa Cruz Biotechnology, Inc.) at 37 °C for 1 and 10 min. The sample mixtures were subsequently analyzed by denaturing PAGE (16% acrylamide, 20% formamide) and visualized using SYBR™ Gold staining.

Intramolecular disulfide crosslinking to form a disulfide-crosslinked stem-loop structure

Chemical oxidation (I_2) and reduction (DTT): a 72-mer ODN strand (0.5 μM) was prepared in phosphate buffer (20 mM, pH 7.0) containing NaCl (100 mM) and DTT (50 μM). Crosslinking was induced by treatment with I_2 (100 μM), and the reaction was incubated at 10 °C for 30 min. Redox cycling was performed three times, maintaining a DTT:I_2 concentration ratio of 2:1 for cleavage and 1:2 for crosslinking.

Photoirradiation and DTT reduction: a 72-mer ODN strand (0.5 μM) was prepared in phosphate buffer (20 mM, pH 7.0) containing NaCl (100 mM) and irradiated with 365 nm LED light (UV intensity: 34.1 W/m^2) for 30 s at 0 °C. The resulting photoinduced crosslinked product was incubated with 100 μM DTT, followed by the addition of 100 μM Py–SS–Py. The solution was then irradiated again using a 365 nm UV LED for 30 s at 0 °C (UV light intensity 3.0 W/m^2).

Reaction mixtures were analyzed by denaturing PAGE (16% acrylamide, 20% formamide) and visualized using SYBR™ Gold staining.

Data availability

The raw data that support the findings of this study are available in the Figshare repository at https://doi.org/10.6084/m9.figshare.30737996.

Received: 5 April 2025; Accepted: 5 December 2025;
Published online: 23 December 2025

References

1. Sessler, J. L., Lawrence, C. M. & Jayawickramarajah, J. Molecular recognition via base-pairing. *Chem. Soc. Rev.* **36**, 314–325 (2007).
2. Craig, M. E., Crothers, D. M. & Doty, P. Relaxation kinetics of dimer formation by self complementary oligonucleotides. *J. Mol. Biol.* **62**, 383–401 (1971).
3. Sugimoto, N. et al. Thermodynamic parameters to predict stability of RNA/DNA hybrid duplexes. *Biochemistry* **34**, 11211–11216 (1995).
4. Sharma, V. K., Sharma, R. K. & Singh, S. K. Antisense oligonucleotides: modifications and clinical trials. *Med. Chem. Commun.* **5**, 1454–1471 (2014).
5. Smith, C. I. E. & Zain, R. Therapeutic oligonucleotides: state of the art. *Annu. Rev. Pharm. Toxicol.* **59**, 605–630 (2019).
6. Wu, Y. Unwinding and rewinding: double faces of helicase? *J. Nucleic Acids* **2012**, 140601 (2012).
7. Neitz, H., Bessi, I., Kuper, J., Kisker, C. & Höbartner, C. Programmable DNA interstrand crosslinking by Alkene–Alkyne [2 + 2] photocycloaddition. *J. Am. Chem. Soc.* **145**, 9428–9433 (2023).
8. Sands, H. et al. Biodistribution and metabolism of internally 3H-labeled oligonucleotides. I. Comparison of a phosphodiester and a phosphorothioate. *Mol. Pharm.* **45**, 932–943 (1994).
9. Ochoa, S. & Milam, V. T. Modified nucleic acids: expanding the capabilities of functional oligonucleotides. *Molecules* **25**, 4659 (2020).
10. Gorska, K. & Winssinger, N. Reactions templated by nucleic acids: more ways to translate oligonucleotide-based instructions into emerging function. *Angew. Chem. Int. Ed.* **52**, 6820–6843 (2013).
11. Onizuka, K., Yamano, Y., Abdelhady, A. M. & Nagatsugi, F. Hybridization-specific chemical reactions to create interstrand crosslinking and threaded structures of nucleic acids. *Org. Biomol. Chem.* **20**, 4699–4708 (2022).
12. Rajendran, A., Endo, M., Katsuda, Y., Hidaka, K. & Sugiyama, H. Photo-cross-linking-assisted thermal stability of DNA origami structures and its application for higher-temperature self-assembly. *J. Am. Chem. Soc.* **133**, 14488–14491 (2011).
13. Brown, T. M., Fakih, H. H., Saliba, D., Asohan, J. & Sleiman, H. F. Stabilization of functional DNA structures with mild photochemical methods. *J. Am. Chem. Soc.* **145**, 2142–2151 (2023).
14. Mie, Y. et al. Function control of anti-microRNA oligonucleotides using interstrand cross-linked duplexes. *Mol. Ther. Nucleic Acids* **10**, 64–74 (2018).
15. Abdelhady, A. M. et al. Synthesis of crosslinked 2′-OMe RNA duplexes and their application for effective inhibition of miRNA function. *Bioorg. Med. Chem. Lett.* **48**, 128257 (2021).
16. Kuper, J. et al. XPD stalled on cross-linked DNA provides insight into damage verification. *Nat. Struct. Mol. Biol.* **31**, 1580–1588 (2024).
17. Noll, D. M., Mason, T. M. & Miller, P. S. Formation and repair of interstrand cross-links in DNA. *Chem. Rev.* **106**, 277–301 (2006).
18. Hashimoto, S., Anai, H. & Hanada, K. Mechanisms of interstrand DNA crosslink repair and human disorders. *Genes Environ.* **38**, 9 (2016).
19. Higuchi, M., Kobori, A., Yamayoshi, A. & Murakami, A. Synthesis of antisense oligonucleotides containing 2′-O-psoralenylmethoxyalkyl adenosine for photodynamic regulation of point mutations in RNA. *Bioorg. Med. Chem.* **17**, 475–483 (2009).
20. Yamayoshi, A. et al. Selective cross-linking behavior of oligodeoxyribonucleotides containing 2′-O-[N-(4,5′,8-trimethylpsoralen-4′-ylmethylcarbamoyl)]adenosine to mutant H-ras DNA. *Nucleosides Nucleotides Nucleic Acids* **39**, 119–130 (2020).
21. Nakao, J. et al. Unique crosslinking properties of psoralen-conjugated oligonucleotides developed by novel psoralen N-hydroxysuccinimide esters. *ChemBioChem* **24**, e202200789 (2023).
22. Sakamoto, T., Tanaka, Y. & Fujimoto, K. DNA photo-cross-linking using 3-cyanovinylcarbazole modified oligonucleotide with threoninol linker. *Org. Lett.* **17**, 936–939 (2015).
23. Fujimoto, K., Yang-Chun, H. & Nakamura, S. Strong inhibitory effects of antisense probes on gene expression through ultrafast RNA photocrosslinking. *Chem. Asian J.* **14**, 1912–1916 (2019).
24. Fujimoto, K. et al. DNA photo-cross-linking using a pyranocarbazole-modified oligodeoxynucleotide with a d-threoninol linker. *RSC Adv.* **9**, 30693–30697 (2019).
25. Yoshimura, Y. & Fujimoto, K. Ultrafast reversible photo-cross-linking reaction: toward in situ DNA manipulation. *Org. Lett.* **10**, 3227–3230 (2008).
26. Qiu, Z., Lu, L., Jian, X. & He, C. A diazirine-based nucleoside analogue for efficient DNA interstrand photocross-linking. *J. Am. Chem. Soc.* **130**, 14398–14399 (2008).
27. Nakamoto, K. & Ueno, Y. Diazirine-containing RNA photo-cross-linking probes for capturing microRNA targets. *J. Org. Chem.* **79**, 2463–2472 (2014).
28. Sugihara, Y., Nakata, Y., Yamayoshi, A., Murakami, A. & Kobori, A. Cross-linking antisense oligodeoxyribonucleotides with a photoresponsive α-chloroaldehyde moiety for RNA point mutations. *J. Org. Chem.* **81**, 981–986 (2016).
29. Sun, H., Fan, H. & Peng, X. Quantitative DNA interstrand cross-link formation by coumarin and thymine: structure determination, sequence effect, and fluorescence detection. *J. Org. Chem.* **79**, 11359–11369 (2014).
30. Haque, M. M., Sun, H., Liu, S., Wang, Y. & Peng, X. Photoswitchable formation of a DNA interstrand cross-link by a coumarin-modified nucleotide. *Angew. Chem. Int. Ed.* **53**, 7001–7005 (2014).
31. Hentschel, S., Alzeer, J., Angelov, T., Schärer, O. D. & Luedtke, N. W. Synthesis of DNA interstrand cross-links using a photocaged nucleobase. *Angew. Chem. Int. Ed.* **51**, 3466–3469 (2012).

32. Stevens, K. & Madder, A. Furan-modified oligonucleotides for fast, high-yielding and site-selective DNA inter-strand cross-linking with non-modified complements †. *Nucleic Acids Res.* **37**, 1555–1565 (2009).
33. Halila, S., Velasco, T., Clercq, P. De & Madder, A. Fine-tuning furan toxicity: fast and quantitative DNA interchain cross-link formation upon selective oxidation of a furan containing oligonucleotide. *Chem. Commun.* 936–938 https://doi.org/10.1039/B415092A (2005)
34. Nagatsugi, F., Kawasaki, T., Usui, D., Maeda, M. & Sasaki, S. Highly efficient and selective cross-linking to cytidine based on a new strategy for auto-activation within a duplex. *J. Am. Chem. Soc.* **121**, 6753–6754 (1999).
35. Onizuka, K. et al. Synthesis of native-like crosslinked duplex RNA and study of its properties. *Bioorg. Med. Chem.* **25**, 2191–2199 (2017).
36. Soemawisastra, N. et al. Uracil-selective cross-linking in RNA and inhibition of miRNA function by 2-amino-6-vinyl-7-deazapurine deoxynucleosides. *ChemBioChem* **25**, e202400417 (2024).
37. Kusano, S. et al. Crosslinking reactions of 4-amino-6-oxo-2-vinylpyrimidine with guanine derivatives and structural analysis of the adducts. *Nucleic Acids Res.* **43**, 7717–7730 (2015).
38. Peng, X., Hong, I. S., Li, H., Seidman, M. M. & Greenberg, M. M. Interstrand cross-link formation in duplex and triplex DNA by modified pyrimidines. *J. Am. Chem. Soc.* **130**, 10299–10306 (2008).
39. Morton, S. B. et al. Efficient synthesis of DNA duplexes containing reduced acetaldehyde interstrand cross-links. *J. Am. Chem. Soc.* **145**, 953–959 (2023).
40. Zeng, Q. & Rokita, S. E. Tandem quinone methide generation for cross-linking DNA. *J. Org. Chem.* **61**, 9080–9081 (1996).
41. Kumar, D., Veldhuyzen, W. F., Zhou, Q. & Rokita, S. E. Conjugation of a hairpin pyrrole-imidazole polyamide to a quinone methide for control of DNA cross-linking. *Bioconjug. Chem.* **15**, 915–922 (2004).
42. Hutchinson, M. A., Deeyaa, B. D., Byrne, S. R., Williams, S. J. & Rokita, S. E. Directing quinone methide-dependent alkylation and cross-linking of nucleic acids with quaternary amines. *Bioconjug. Chem.* **31**, 1486–1496 (2020).
43. Ye, M. et al. Site-specific inter-strand cross-links of DNA duplexes. *Chem. Sci.* **4**, 1319–1329 (2013).
44. Dutta, S., Chowdhury, G. & Gates, K. S. Interstrand cross-links generated by abasic sites in duplex DNA. *J. Am. Chem. Soc.* **129**, 1852–1853 (2007).
45. Nejad, M. I. et al. Interstrand DNA cross-links derived from reaction of a 2-aminopurine residue with an abasic site. *ACS Chem. Biol.* **14**, 1481–1489 (2019).
46. Tomás-Gamasa, M., Serdjukow, S., Su, M., Müller, M. & Carell, T. "Post-It" type connected DNA created with a reversible covalent cross-link. *Angew. Chem. Int. Ed.* **54**, 796–800 (2015).
47. Kočalka, P., El-Sagheer, A. H. & Brown, T. Rapid and efficient DNA strand cross-linking by click chemistry. *ChemBioChem* **9**, 1280–1285 (2008).
48. Nakane, M., Ichikawa, S. & Matsuda, A. Triazole-linked dumbbell oligodeoxynucleotides with NF-κB binding ability as potential decoy molecules. *J. Org. Chem.* **73**, 1842–1851 (2008).
49. Kashida, H., Doi, T., Sakakibara, T., Hayashi, T. & Asanuma, H. p-stilbazole moieties as artificial base pairs for photo-cross-linking of DNA duplex. *J. Am. Chem. Soc.* **135**, 7960–7966 (2013).
50. Onizuka, K., Ishida, K., Mano, E. & Nagatsugi, F. Alkyne–alkyne photo-cross-linking on the flipping-out field. *Org. Lett.* **21**, 2833–2837 (2019).
51. Abdelhady, A. M. et al. Rapid alkene–alkene photo-cross-linking on the base-flipping-out field in duplex DNA. *J. Org. Chem.* **87**, 2267–2276 (2022).
52. Kashida, H., Azuma, H., Sotome, H., Miyasaka, H. & Asanuma, H. Site-selective photo-crosslinking of stilbene pairs in a DNA duplex mediated by ruthenium photocatalyst. *Angew. Chem. Int. Ed.* **63**, e202319516 (2024).
53. Stasińska, A. R., Putaj, P. & Chmielewski, M. K. Disulfide bridge as a linker in nucleic acids' bioconjugation. Part II: a summary of practical applications. *Bioorg. Chem.* **95**, 103518 (2020).
54. Benezra, R. An intermolecular disulfide bond stabilizes E2A homodimers and is required for DNA binding at physiological temperatures. *Cell* **79**, 1057–1067 (1994).
55. Manteca, A. et al. The influence of disulfide bonds on the mechanical stability of proteins is context dependent. *J. Biol. Chem.* **292**, 13374–13380 (2017).
56. Liu, T. et al. Enhancing protein stability with extended disulfide bonds. *Proc. Natl. Acad. Sci. USA* **113**, 5910–5915 (2016).
57. Shaked, Z., Szajewski, R. P. & Whitesides, G. M. Rates of thiol-disulfide interchange reactions involving proteins and kinetic measurements of thiol pKa values. *Biochemistry* **19**, 4156–4166 (1980).
58. Cremers, C. M. & Jakob, U. Oxidant sensing by reversible disulfide bond formation*. *J. Biol. Chem.* **288**, 26489–26496 (2013).
59. Wang, B. et al. Base-sequence-independent efficient redox switching of self-assembled DNA nanocages. *ChemBioChem* **20**, 2743–2746 (2019).
60. Shokri, E. et al. Disulfide-induced self-assembled targets: a novel strategy for the label free colorimetric detection of DNAs/RNAs via unmodified gold nanoparticles. *Sci. Rep.* **7**, 45837 (2017).
61. Saran, R., Huang, Z. & Liu, J. Phosphorothioate nucleic acids for probing metal binding, biosensing and nanotechnology. *Coord. Chem. Rev.* **428**, 213624 (2021).
62. Wolfrum, M., Schwarz, R. J., Schwarz, M., Kramer, M. & Richert, C. Stabilizing DNA nanostructures through reversible disulfide crosslinking. *Nanoscale* **11**, 14921–14928 (2019).
63. Faiad, S. et al. Site-specific disulfide-mediated crosslinking of DNA nanocubes for enhanced biological applications. *Small Sci.* **15**, 2400471 (2024).
64. Torres, A. G. & Gait, M. J. Exploiting cell surface thiols to enhance cellular uptake. *Trends Biotechnol.* **30**, 185–190 (2012).
65. Huang, C.-R., Chang, C.-H., Su, Y.-C., Tseng, T.-J. & Chen, Y.-F. Organic disulfide crosslinked nucleic acid-based nanocarriers for anticancer drug applications. *J. Drug Deliv. Sci. Technol.* **86**, 104643 (2023).
66. De Stefano, M. & Vesterager Gothelf, K. Dynamic chemistry of disulfide terminated oligonucleotides in duplexes and double-crossover tiles. *ChemBioChem* **17**, 1122–1126 (2016).
67. Bauhuber, S., Hozsa, C., Breunig, M. & Göpferich, A. Delivery of nucleic acids via disulfide-based carrier systems. *Adv. Mater.* **21**, 3286–3306 (2009).
68. Beuck, C. & Weinhold, E. Reversibly locked thionucleobase pairs in DNA to study base flipping enzymes. *Beilstein J. Org. Chem.* **10**, 2293–2306 (2014).
69. Beddows, A. et al. Interstrand disulfide crosslinking of DNA bases supports a double nucleotide unpairing mechanism for flap endonucleases. *Chem. Commun.* **48**, 8895–8897 (2012).
70. Hatano, A., Okada, M. & Kawai, G. Solution structure of S-DNA formed by covalent base pairing involving a disulfide bond. *Org. Biomol. Chem.* **10**, 7327–7333 (2012).
71. Ono, A. et al. Crystal structure of a DNA duplex cross-linked by 6-thioguanine–6-thioguanine disulfides: reversible formation and cleavage catalyzed by Cu(ii) ions and glutathione. *RSC Adv.* **9**, 22859–22862 (2019).
72. Lunn, S. M. L. et al. Duplex healing of selectively thiolated guanosine mismatches through a Cd2+ chemical stimulus. *ChemBioChem* **19**, 1115–1118 (2018).
73. Kazumitsu Onizuka, Y. T. & Sasaki, S. A new odorless procedure for the synthesis of 2′-deoxy-6-thioguanosine and its incorporation into

oligodeoxynucleotides. *Nucleosides Nucleotides Nucleic Acids* **28**, 752–760 (2009).
74. Coleman, R. S., McCary, J. L. & Perez, R. J. Thionucleoside disulfides as covalent constraints of DNA conformation. *Tetrahedron* **55**, 12009–12022 (1999).
75. Ashwood, B., Pollum, M. & Crespo-Hernández, C. E. Photochemical and photodynamical properties of sulfur-substituted nucleic acid bases. *Photochem. Photobio.* **95**, 33–58 (2019).
76. Brem, R., Daehn, I. & Karran, P. Efficient DNA interstrand crosslinking by 6-thioguanine and UVA radiation. *DNA Repair* **10**, 869–876 (2011).
77. Brem, R. & Karran, P. Multiple forms of DNA damage caused by UVA photoactivation of DNA 6-thioguanine. *Photochem. Photobio.* **88**, 5–13 (2012).
78. Brem, R., Guven, M. & Karran, P. Oxidatively-generated damage to DNA and proteins mediated by photosensitized UVA. *Free Radic. Biol. Med.* **107**, 101–109 (2017).
79. Gueranger, Q., Kia, A., Frith, D. & Karran, P. Crosslinking of DNA repair and replication proteins to DNA in cells treated with 6-thioguanine and UVA. *Nucleic Acids Res.* **39**, 5057–5066 (2011).
80. Favre, A., Saintomé, C., Fourrey, J.-L., Clivio, P. & Laugâa, P. Thionucleobases as intrinsic photoaffinity probes of nucleic acid structure and nucleic acid-protein interactions. *J. Photochem. Photobio. B* **42**, 109–124 (1998).
81. Nishioka, T., Oshiro, I., Onizuka, K., Taniguchi, Y. & Sasaki, S. Efficient thymidine-selective DNA interstrand photo-activated crosslinking by the 6-thioguanine connected *via* an ethylene-linker to the 2′-deoxyribose unit. *Chem. Pharm. Bull.* **64**, 1315–1320 (2016).
82. Vorlíčková, M., Kejnovská, I., Bednářová, K., Renčiuk, D. & Kypr, J. Circular dichroism spectroscopy of DNA: from duplexes to quadruplexes. *Chirality* **24**, 691–698 (2012).
83. Visone, V. et al. Topoisomerases inhibition and DNA binding mode of daunomycin–oligoarginine conjugate. *J. Enzym. Inhib. Med. Chem.* **35**, 1363–1371 (2020).
84. Guo, C. et al. DNA interstrand crosslinks by H-pin polyamide (S)-seco-CBI conjugates. *ChemBioChem* **18**, 166–170 (2017).
85. Oh, D. H., Suzara, V. & Krishnan, R. Modulation of psoralen DNA crosslinking kinetics associated with a triplex-forming oligonucleotide. *Photochem. Photobio.* **84**, 727–733 (2008).
86. Ruhayel, R. A. et al. Factors affecting DNA–DNA interstrand cross-links in the antiparallel 3′–3′ sense: a comparison with the 5′–5′ directional isomer. *Chem. A Eur. J.* **15**, 9365–9374 (2009).
87. Amin, S. B. M. et al. Effects of local sequence, reaction conditions, and various additives on the formation and stability of interstrand cross-links derived from the reaction of an abasic site with an adenine residue in duplex DNA. *ACS Omega* **7**, 36888–36901 (2022).
88. Rozelle, A. L., Cheun, Y., Vilas, C. K., Koag, M.-C. & Lee, S. DNA interstrand cross-links induced by the major oxidative adenine lesion 7,8-dihydro-8-oxoadenine. *Nat. Commun.* **12**, 1897 (2021).
89. Huskova, A., Landova, B., Boura, E. & Silhan, J. The rate of formation and stability of abasic site interstrand crosslinks in the DNA duplex. *DNA Repair* **113**, 103300 (2022).
90. Steenken, S. & Jovanovic, S. V. How easily oxidizable Is DNA? One-electron reduction potentials of adenosine and guanosine radicals in aqueous solution. *J. Am. Chem. Soc.* **119**, 617–618 (1997).
91. Fröbel, S., Levi, L., Ulamec, S. M. & Gilch, P. Photoinduced electron transfer between Psoralens and DNA: influence of DNA sequence and substitution. *ChemPhysChem* **17**, 1377–1386 (2016).
92. Cesaretti, A. et al. Direct observation of guanine photo-oxidation from new potential anticancer drugs via ultrafast electron transfer. *Mater. Adv.* **5**, 7650–7658 (2024).
93. Zgarbová, M., Otyepka, M., Šponer, J., Lankaš, F. & Jurečka, P. Base pair fraying in molecular dynamics simulations of DNA and RNA. *J. Chem. Theory Comput.* **10**, 3177–3189 (2014).
94. Mai, S. et al. The origin of efficient triplet state population in sulfur-substituted nucleobases. *Nat. Commun.* **7**, 13077 (2016).
95. Zhang, X. et al. Novel DNA lesions generated by the interaction between therapeutic thiopurines and UVA light. *DNA Repair* **6**, 344–354 (2007).
96. Ren, X. et al. Guanine sulphinate is a major stable product of photochemical oxidation of DNA 6-thioguanine by UVA irradiation. *Nucleic Acids Res.* **38**, 1832–1840 (2010).
97. Zou, X., Zhao, H., Yu, Y. & Su, H. Formation of guanine-6-sulfonate from 6-thioguanine and singlet oxygen: a combined theoretical and experimental study. *J. Am. Chem. Soc.* **135**, 4509–4515 (2013).
98. Zhang, Y., Zhu, X., Smith, J., Haygood, M. T. & Gao, R. Direct observation and quantitative characterization of singlet oxygen in aqueous solution upon UVA excitation of 6-thioguanines. *J. Phys. Chem. B* **115**, 1889–1894 (2011).
99. Zhang, Y., Barnes, A. N., Zhu, X., Campbell, N. F. & Gao, R. Quantification of thiopurine/UVA-induced singlet oxygen production. *J. Photochem. Photobio. A Chem.* **224**, 16–24 (2011).
100. Euceda, N. et al. Thioguanine restoration through type I photosensitization-superoxide oxidation-glutathione reduction cycles. *Phys. Chem. Chem. Phys.* **23**, 5069–5073 (2021).
101. Alam, M. M., Fujitsuka, M., Watanabe, A. & Ito, O. Photochemical properties of excited triplet state of 6H-purine-6-thione investigated by laser flash photolysis. *J. Phys. Chem. A* **102**, 1338–1344 (1998).
102. Dong, J. et al. Free-radical-mediated photoinduced electron transfer between 6-thioguanine and tryptophan leading to DNA–protein-like cross-link. *J. Phys. Chem. B* **126**, 14–22 (2022).
103. Gomzi, V. & Herak, J. N. Ionization potentials of nucleobase analogs using partial third-order electron propagator method. *J. Mol. Struct. THEOCHEM* **683**, 155–157 (2004).
104. Liu, R., Fu, S., Zhan, H. & Lucia, L. A. General spectroscopic protocol to obtain the concentration of the superoxide anion radical. *Ind. Eng. Chem. Res* **48**, 9331–9334 (2009).
105. Zhang, Y., Dai, M. & Yuan, Z. Methods for the detection of reactive oxygen species. *Anal. Methods* **10**, 4625–4638 (2018).
106. Shu, Z. et al. Disulfide-unit conjugation enables ultrafast cytosolic internalization of antisense DNA and siRNA. *Angew. Chem. Int. Ed.* **58**, 6611–6615 (2019).
107. Li, J. et al. Self-assembly of DNA nanohydrogels with controllable size and stimuli-responsive property for targeted gene regulation therapy. *J. Am. Chem. Soc.* **137**, 1412–1415 (2015).
108. Wang, C., Fadeev, M., Vázquez-González, M. & Willner, I. Stimuli-responsive donor–acceptor and DNA-crosslinked hydrogels: application as shape-memory and self-healing materials. *Adv. Funct. Mater.* **28**, 1803111 (2018).
109. Dutta, K., Das, R., Medeiros, J. & Thayumanavan, S. Disulfide bridging strategies in viral and nonviral platforms for nucleic acid delivery. *Biochemistry* **60**, 966–990 (2021).

Acknowledgements

We thank the Tagen Central Analytical Facility and the support program for young researchers from Tohoku University Technical Support Center for supporting NMR, ESI-HRMS, and MALDI-TOF MS measurements. This work was supported in part by Scientific Research on Transformative Research Areas (A) “Biophysical Chemistry for Material Symbiosis” (No. JP23H04051 to K.O.) and Grant-in-Aid for Scientific Research (B) (No. JP24K01641 to K.O. and No. JP23H02076 to F.N.) from the Japan Society for the Promotion of Science (JSPS); the Japan Science and Technology Agency (JST) FOREST program (No. JPMJFR2002 to K.O.); and the research program of the Crossover Alliance to Create the Future with People, Intelligence and Materials from MEXT, Japan. The first author (J.A.O.) gratefully acknowledges the financial support provided by a full scholarship from the Ministry of Education, Culture, Sports, Science, and Technology (MEXT) of Japan and expresses her sincere appreciation for this support.

Author contributions

K.O. and J.A.O. designed the experiments. J.A.O. synthesized compounds and oligo DNAs. Analytical experiments were primarily performed by J.A.O., with contributions from Y.Y. The manuscript was primarily written by J.A.O. and K.O. K.O. and F.N. mentored the research. All authors discussed the results and provided feedback on the study and manuscript.

Competing interests

The authors declare no competing interests.

Additional information

Supplementary information The online version contains supplementary material available at https://doi.org/10.1038/s42004-025-01853-z.

Correspondence and requests for materials should be addressed to Kazumitsu Onizuka or Fumi Nagatsugi.

Peer review information *Communications Chemistry* thanks Annemieke Madder, Natalia Y. Tretyakova, Gertjan Colpaert and the other, anonymous, reviewer(s) for their contribution to the peer review of this work. A peer review file is available.